THE PENNSYLVANIA STATE UNIVERSITY
SCHREYER HONORS COLLEGE

DEPARTMENT OF CHEMISTRY

SYNTHESIS OF OLIGOMERIC RUTHENIUM POLYPYRIDYL DYES AND LIQUID IMIDAZOLIUM ZWITTERIONS FOR IMPROVED ENERGY GENERATION AND STORAGE

AUGUST J. ROTHENBERGER
SPRING 2020

A thesis
submitted in partial fulfillment
of the requirements
for a baccalaureate degree in Chemistry
with honors in Chemistry

Reviewed and approved* by the following:

Thomas E. Mallouk
Evan Pugh Professor of Chemistry, Professor Emeritus
Thesis Supervisor

Raymond L. Funk
Professor of Chemistry
Honors Advisor

Robert J. Hickey
Assistant Professor of Materials Science and Engineering
Faculty Reader

* Signatures are on file in the Schreyer Honors College.

ABSTRACT

Water-splitting, dye-sensitized photoelectrochemical cells (WS-DSPECs) use molecular sensitizers to harvest solar energy and facilitate the catalytic reactions necessary to generate hydrogen and oxygen from water. Photostability of sensitizers and cross-surface hole diffusion on the electrode surface are two properties that have received recent attention as key limiting factors in the efficiency of WS-DSPECs. We have synthesized a novel oligomeric ruthenium polypyridyl dye that has dramatically improved adhesion to TiO_2 electrodes at pH 4.8 and pH 7.8. Long-term stability of the oligomer was observed at high pH ranges traditionally incompatible with monomeric dyes. The apparent hole diffusion constant, D_{app}, of the oligomer was an order of magnitude higher than the monomeric dye, indicating the oligomer's effectiveness in enhancing cross-surface transport of oxidizing equivalents to water-splitting catalytic sites. These results demonstrate that use of oligomeric dyes is an effective strategy in designing high-stability chromophores for WS-DSPECs.

In the pursuit of solid-state, solvent-free lithium ion batteries, polyelectrolytes have gained considerable attention. Zwitterions with large static dielectric constants have been shown to dramatically increase ionic conductivity in polyelectrolytes by enhancing ion dissociation from the polymer backbone. Low-melting temperature zwitterions mitigate complications caused by addition of a solid molecule to the conductive polymer system. Additionally, it is possible to directly measure the static dielectric constant, ε_s, of the pure liquid zwitterions at room temperature. We have successfully synthesized two imidazolium sulfonate zwitterions, **OE_2ImPS** and **OE_2ImBS**, the latter of which is a novel molecule, which display glass transitions well below room temperature (T_g = -9.75 and -10.75, respectively) and exceptionally high static dielectric constants (ε_s = 204.8 and 205.1 at 20 °C). These findings indicate that the synthesized zwitterions should be highly effective at increasing ionic conductivity in polyelectrolytes.

TABLE OF CONTENTS

LIST OF FIGURES

LIST OF TABLES

ACKNOWLEDGEMENTS

The completion of this thesis would not have been possible without the support and guidance of many individuals. I would like to thank my thesis advisor Prof. Tom Mallouk for welcoming me into his lab as a freshman, providing resources to complete my thesis research, and supervising me throughout my undergraduate career. Additionally, I must thank my graduate student mentor Chris Gray for providing invaluable insights into the research process, guiding me through the oligomer project, and his assistance in writing Chapter 1. This material is based upon work supported by the US Department of Energy under Award No. DE-FG02-07ER15911. Any opinions, findings, and conclusions or recommendations expressed in this publication are those of the author and do not necessarily reflect the views of the DOE.

I must also thank Prof. Rob Hickey for allowing me to join his lab during my junior year to learn more about materials science and for his guidance throughout my research progress. I would like to thank my graduate student mentor Wenwen Mei for her assistance during synthesis and while writing this report as well as fellow undergraduate Josh Rinehart for his experimental guidance. Financial support was provided through Penn State research faculty startup funds and the National Science Foundation under grant DMR: 1807934.

I am extremely grateful for personal support received from the Penn State Department of Chemistry through the John and Elizabeth Holmes Teas Scholarship as well as from the Schreyer Honors College. I would additionally like to thank Prof. Ray Funk and Prof. Kate Masters for providing helpful advising support throughout my undergraduate career and planning for future education through graduate school.

Finally, I would like to thank my parents for sparking my interest in science as well as their continued unconditional love and support as I pursue a career in chemistry.

PREFACE

The research included in the following thesis was completed in two laboratories and represents two fields of study I explored during my undergraduate career. In May 2020 I will graduate with a B.S. in Chemistry and a minor in Polymer Science; Chapter 1 highlights my experience in the Department of Chemistry while Chapter 2 describes a project in the field of Materials Science and Engineering. Both projects are joined through the fields of energy science: Chapter 1 involves the field of energy generation via solar-driven conversion of water to hydrogen gas, Chapter 2 relates to the use of ion conductive polymers in next-generation lithium-ion batteries. This wide lens through which I have approached the field of energy science will likely prove useful as continue my education in graduate school.

The work included in Chapter 1, "A Ruthenium Polypyridyl Oligomer to Improve Water-Splitting Dye-Sensitized Photoelectrochemical Cells," was conducted in the laboratory of Thomas E. Mallouk, who is a Professor Emeritus of Chemistry at Penn State and a Vagelos Professor in Energy Research and Professor of Chemistry at the University of Pennsylvania. The research incorporates the fields of organometallic synthesis, materials chemistry, and electrochemistry in the synthesis and analysis of a novel dye molecule to use at the photoanode of water-splitting devices. Continued development of these photoelectrochemical devices may eventually lead to their widespread adoption to renewably generate clean burning hydrogen gas as an energy source. The projects I directly worked on in the Mallouk group are described in this thesis; the full results of the study are published in the *Journal of Physical Chemistry C*.[1]

Research included in Chapter 2, "Liquid Imidazolium Zwitterions to Improve the Conductivity of Lithium Ion Battery Polyelectrolytes," was performed in the laboratory of Robert J. Hickey, an Assistant Professor of Materials Science and Engineering at Penn State. The project

involved the synthesis and study of low melting temperature zwitterions with high dielectric constants. The overarching theme in Chapter 2 is the development of solid-state polyelectrolytes to eliminate the use of dangerous organic solvents in lithium ion batteries. Other concepts explored include the emerging usage of zwitterions as ionic conductivity enhancers, the effect of molecular structure on a zwitterion's glass transition temperature and static dielectric constant, as well as the comparison of different anions in otherwise equivalent zwitterions.

Chapter 1

A Ruthenium Polypyridyl Oligomer to Improve Water-Splitting Dye-Sensitized Photoelectrochemical Cells

1.1 Introduction

1.1.1 Photoelectrochemical Cells

The ability to harness the unlimited power of the sun to meet increasing energy demands has long been a goal of scientists. If it were possible to cover only 1% of land on earth with 10% efficient solar capture devices, the energy would generate 36 TW of power per year–the global energy consumption predicted until at least 2050.[2] One approach to achieving this goal is to develop biomimetic devices capable of replicating nature's photosynthetic pathways. Water-splitting, dye-sensitized photoelectrochemical cells (WS-DSPECs) harvest sunlight using molecular sensitizers and use the energy to split water into oxygen and hydrogen gas. The storage of renewable energy in the form of hydrogen and liquid fuels will be an important factor in preventing the rise of atmospheric carbon dioxide emissions from conventional fossil fuel burning in the near future. Hydrogen generated using WS-DSPECs could be used as a clean energy source with the only emission being water vapor. Additionally, hydrogen gas can be stored effectively and densely,[3] rectifying energy loss pathways present in other renewables that generate electricity which must be immediately sent into the grid or stored in batteries.

The research of photoelectrochemical systems began with the observation of the Honda-Fujishima effect, where irradiation of the semiconductor TiO_2 enabled splitting of water into hydrogen and oxygen gas with a small applied external potential.[4] A simple photoelectrochemical cell could be constructed by submerging TiO_2 and a platinum counter electrode in water. When the

TiO_2 anode is exposed to sunlight, electron promotion to the conduction band forms holes in the valence band and creates a potential of 3.2 V across the band gap (Equation 1-1).

$$TiO_2 + h\nu \longrightarrow e^- + h^+ \quad (1\text{-}1)$$

The created potential is capable of facilitating the oxygen evolution reaction (OER), defined by Equation 1-2, which requires an overall potential of 1.23 V between two electrodes. The holes created in the valence band of TiO_2 are thus quenched using electrons generated from splitting of water.

$$2H_2O + 4h^+ \rightarrow O_2 + 4H^+ \quad (1\text{-}2)$$

Since the promoted electrons in TiO_2 are now displaced, they flow across the cell to the platinum cathode and are used to facilitate the hydrogen evolution reaction, reducing protons to hydrogen gas (Equation 1-3). The balanced redox reaction for the photoelectrochemical cell (Equation 1-4) defines water splitting.

$$2H^+ + 2e^- \rightarrow H_2 \quad (1\text{-}3)$$

$$2H_2O + 4h\nu \rightarrow O_2 + 2H_2 \quad (1\text{-}4)$$

Many semiconducting materials including hematite (α-Fe_2O_3),[5] $BiVO_4$,[6,7] CdS,[2] tantalum nitrides such as TaON and Ta_3N_5,[7] and tungstates such as $CuWO_4$ and Fe_2WO_6,[8] have since been analyzed as absorbers in photoelectrochemical systems with various advantages and drawbacks. TiO_2 in the anatase morphology is still largely considered one of the better prospects for photoelectrochemical water splitting due to the well-rounded traits of efficient photoactivity, high stability in acidic and basic conditions,[2] low cost, and nontoxicity to humans.[4] However, the wide band gap of 3.2 eV require that photons have a wavelength less than 387 nm to facilitate the electron transition event, limiting the percentage of the solar spectrum that can be absorbed to 5%.[2] TiO_2 systems thus have a very low maximum solar-to-hydrogen (STH) efficiency, measured as

hydrogen evolved at a specific photocurrent density. Anatase TiO_2 has a meager theoretical STH of 1.3%,[2] which does not meet the US Department of Energy's STH target of least 10% for photoelectrochemical water splitting devices to be commercially viable and competitive with other renewables.[9]

1.1.2 Dye-Sensitization for Water-Splitting

While efforts have been made to dope TiO_2 with carbon, nitrogen, sulfur, and iron to extend its range into the visible regions,[10,11] few significant changes to photoelectrochemical water splitting ability have been realized. Another strategy is the attachment of sensitizers capable of absorbing a larger portion of the solar spectrum to the photoanode. Sensitizers are molecular dyes which have a long-lived excited state able to inject an electron into the conduction band of TiO_2. Grätzel and co-workers successfully implemented the strategy in the design of dye-sensitized solar cells (DSSCs) which convert incident photons to an electric current through facilitation of redox shuttling in I_3^-/I^- solution.[12] WS-DSPECs could be considered aqueous DSSCs where the anode is coupled to a water oxidation catalyst to facilitate the OER. However, while DSSCs have been optimized extensively and can reach power conversion efficiencies of nearly 15%,[13] WS-DSPECs have struggled to break 1% efficiency.[14] The kinetically demanding water oxidation reaction is slow and the aqueous electrolyte introduces stability issues that are much less pronounced in DSSCs.

A diagram depicting electron transport in a WS-DSPEC is shown in Figure 1. To define terminology, oxidizing equivalents (holes) are formed by the absence of an electron and travel in the opposite direction as electrons. The catalytic cycle begins when an incident photon is absorbed by the sensitizer. The excited-state sensitizer then injects an electron into the conduction band of

TiO_2; the now oxidized sensitizer receives an electron from the OER catalyst. The catalyst must be capable of reaching a high oxidation state; four oxidizing equivalents must be transferred to the catalyst from oxidized dye molecules to generate one oxygen molecule from water. Colloidal iridium dioxide is a robust and highly active OER catalyst used by the Mallouk group.[15] Electron recombination occurs if the oxidizing equivalent is transferred to the TiO_2 conduction band from the sensitizer rather than to an OER catalyst. Recombination is a major source of inefficiency in WS-DSPECs and is often the dominant electron transport kinetic pathway, occurring on the time scale of hundreds of microseconds.[16] Optimizing photoanode architecture to reduce recombination is a popular area of research to increase effectiveness of WS-DSPECs.

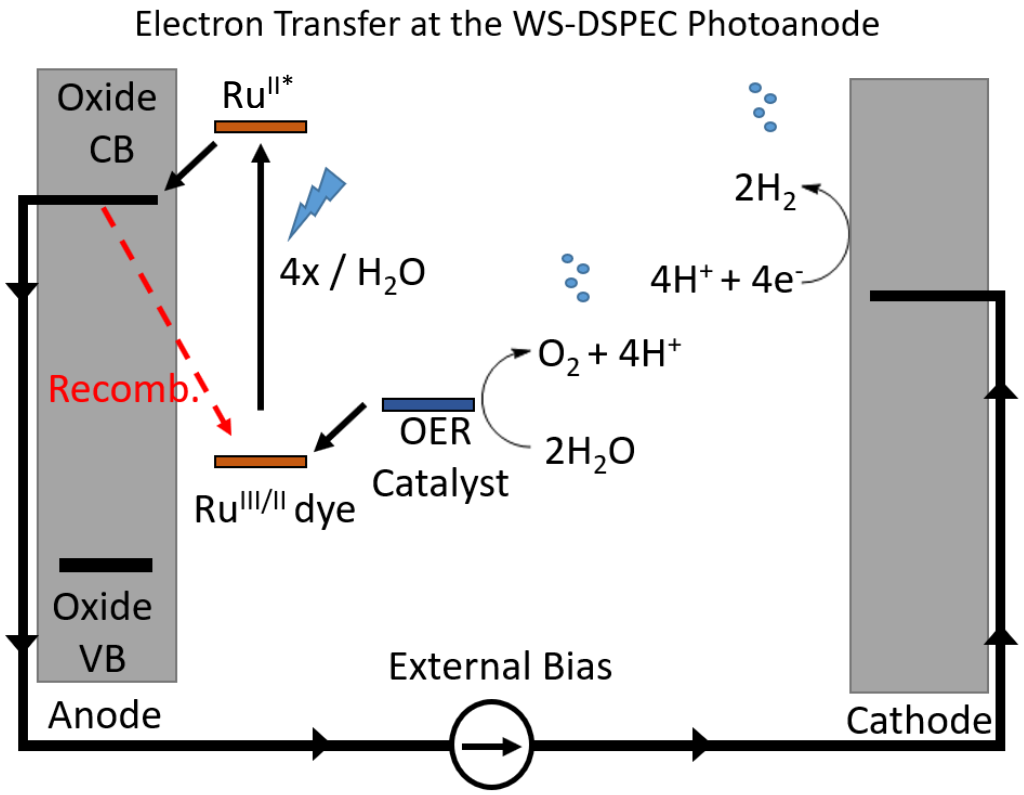

Figure 1. Simplified electron transport in a WS-DSPEC. Light absorption by a molecular sensitizer (Ru^{II}) transfers an electron to the conduction band of TiO_2 where it is transported to the cathode to reduce protons. The oxidized sensitizers then regain electrons from the water splitting reaction.

1.1.3 Challenges Faced by Ruthenium Bipyridyl WS-DSPEC Systems

Previous studies of WS-DSPECs have primarily utilized a derivative of tris(2,2'-bipyridine)ruthenium(II) with a pair of phosphonate anchoring groups at the 4,4' position of one bipyridine ligand, $[Ru(bpy)_2(4,4\text{-}PO_3H_2)_2bpy)]^{2+}$ (**RuP**),[14,17,18] although porphyrins,[19] perylene diimides,[20] and triarylamine dye systems[21] have also been incorporated into water splitting systems. Ruthenium bipyridyl dyes are advantageous due to their intense metal-to-ligand charge transfer (MLCT) absorption[22] and long lived ^{3}MLCT state lasting hundreds of nanoseconds,[23,24] allowing for effective injection into the TiO_2 conduction band.

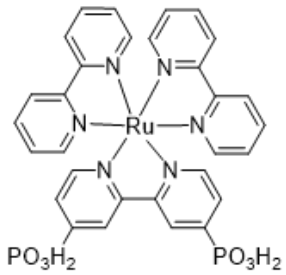

Figure 2. Structure of $[Ru(bpy)_2(4,4\text{-}PO_3H_2)_2bpy)]^{2+}$ (RuP).

One of the major challenges when designing WS-DSPECs is sensitizer instability. The ideal anchor group must be oxidation resistant across a range of pH conditions, effectively bond the sensitizer to TiO_2, and facilitate electron injection from an excited sensitizer to TiO_2. Due to these constraints, carboxylic acid, phosphonic acid, hydroxamic acid, and silatranes are among the few anchor groups that have been used to secure sensitizers at the photoanode.[25] The phosphonate anchoring group trades increased stability for decreased efficiency of electron injection. Despite the stability of phosphonate anchor groups, dye desorption from the electrode surface is still a major factor compromising the lifetime of WS-DSPECs.[14,17,25] The US Department of Energy set the target for photoelectrochemical cells to have a lifetime of at least 5000 hours;[9] sensitizers require significantly increased optimization before that goal is reached.

Efficient charge transfer across the surface of the photoanode must be ensured to limit inefficiency through recombination pathways. Previous studies have shown that each OER catalytic site effectively draws holes only from ruthenium centers nearby it; however, catalysts are typically sparsely distributed on the photoanode surface (on the order of pmol/cm^2).[16] Therefore, only a fraction of the dye coated surface contributes to the water splitting catalytic cycle; many of the oxidized sensitizers are instead quenched through recombination. However, sensitizers that are distant from catalyst sites can still contribute oxidizing equivalents to the catalyst through a cross-surface hole hopping mechanism between nearby ruthenium centers (pathway xi in Figure 3). Recent work has identified the rate of cross-surface hole diffusion as one of the limiting factors in catalytic turnover of these cells.[16,26,27] If hole diffusion is rapid enough, distant dye molecules contribute oxidizing equivalents to the catalyst. If the hole diffusion is slow, then most of the absorbed light energy is not transferred to the catalytic reaction. Designing dyes with improved hole diffusion should correspondingly enhance photoanode activity and efficiency.

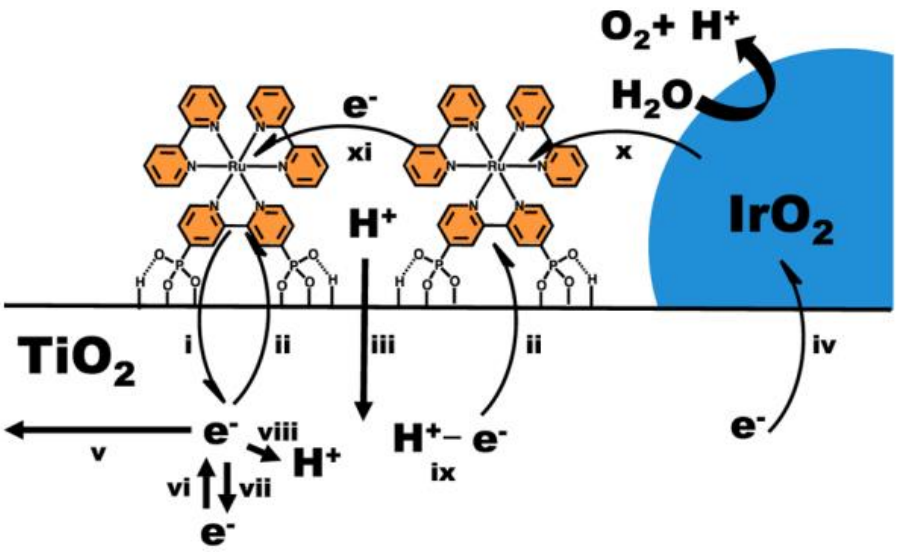

Figure 3. Charge transfer pathways at the photoanode. IrO_2 is an OER catalyst. (i) injection, (ii) recombination, (iii) proton intercalation, (iv) electron scavenging by IrO_2, (v) electron transport to FTO, (vi,vii) reversible detrapping/trapping, (viii)trapping of an

electron at a proton-stabilized site, (ix)proton-stabilized trap state, (x) regeneration of Ru(III), (xi) cross surface hole transport (Reproduced from Ref. [16])

1.1.4 Summary and Significance of Project

Many groups have attempted to exploit the increased stability of polymers to improve lifetimes of DSSCs[28] and WS-DSPECs. Some techniques include the deposition of polymeric dyes,[29] polymerization of dyes after deposition,[30–32] encasing molecular dyes in a polymer overlayer[33,34] or encasing dyes in a metal oxide shell.[18,35–37] These attempts generally increase cell lifetime but tend to vastly complicate sensitizer deposition techniques when constructing photoanodes. Additionally, since the hole diffusion constant is largely determined by the distance between ruthenium centers,[26,27] covalent polymer linkages should be ideal for more effective hole diffusion. Use of a short chain (less than 10 repeat units) oligomeric dye might provide the advantageous aspects of polymeric dyes but would simplify deposition since the sensitizer would likely behave as a small molecule in solution.

The goal of this project was to synthesize and analyze a novel phosphonated oligomeric ruthenium dye (**[RuP]$_n$**) in order to improve the photostability and cross-surface hole diffusion at the anode of a WS-DSPEC. The light-absorbing metal centers in the oligomer are covalently linked before deposition and thereby guaranteed to be a certain distance from each other on the electrode surface. Holes should be transferred more quickly between individual dye complexes than for monomeric dyes, resulting in an improvement to cross-surface hole diffusion. Additionally, incorporating more phosphonate anchor groups per dye molecule should significantly increase attachment points to the TiO_2 surface, thereby enhancing the photostability of the sensitizer.

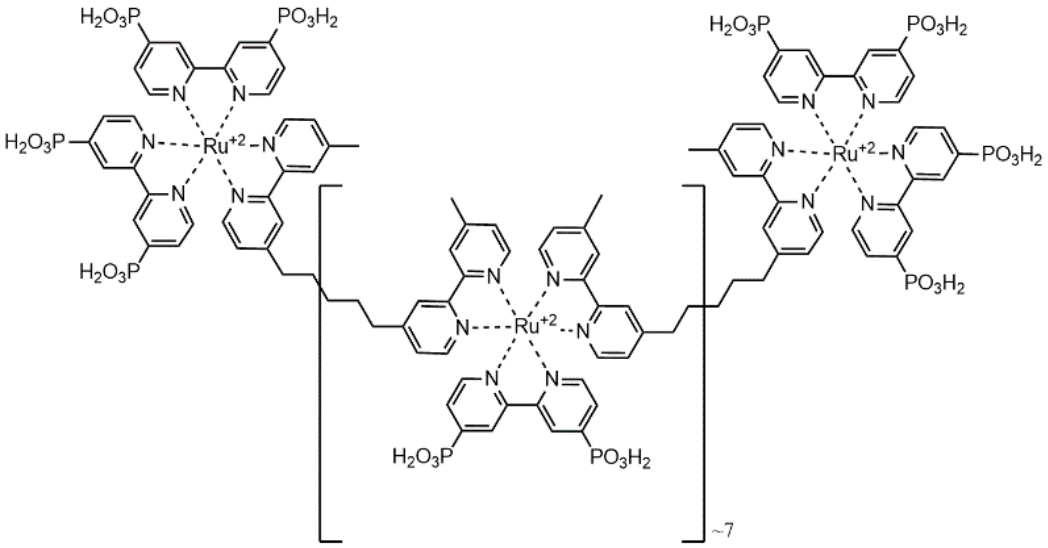

Figure 4. Structure of the phosphonated oligomeric ruthenium bipyridyl sensitizer ([RuP]$_n$)

1.2 Synthesis of RuP and $[RuP]_n$

The 4,4'-bis(diethylphosphonate)-2,2'-bipyridine ligand, $(4,4\text{-}PO_3Et_2)_2bpy$, was purchased from Carbosynth and used without further purification. The monomer, bis(2,2-bipyridine)(4,4-diphosphonato-2,2-bipyridine)-ruthenium bromide, $[Ru(bpy)_2(4,4\text{-}PO_3H_2)_2bpy)]^{2+}$ (**RuP**), was prepared according to literature.[38] The synthesis of **$[RuP]_n$** was performed using a supramolecular polymerization method depicted in Figure 5.

Synthesis of Oligomeric Dye ($[RuP]_n$). Dichlorotetrakis(dimethylsulfoxide) ruthenium(II)[39] and 1,5-bis-(4-methyl-2,2-bipyridyl-4-yl)pentane linker[15,40] were prepared using literature methods. The pentane linker was purified by recrystallization from hot t-butyl methyl ketone. $Ru(DMSO)_4Cl_2$ (0.20 g, 0.40 mmol) and 1,5-bis(4-methyl-2,2-bipyridyl-4-yl)pentane (0.17 g, 0.40 mmol) were added to 50 mL of chloroform and refluxed under argon for 1.5 h. Removing the solvent under reduced pressure yielded a dark brown oil which was dissolved in a mixture of 10 mL of H_2O/15 mL of ethanol. $(4,4\text{-}PO_3Et_2)_2bpy$ (0.10 g, 0.64 mmol) was added, and the solution was refluxed for 2.5 h to yield a clear, dark-red solution. The solvent was reduced to about 10 mL by rotary evaporation, then the product was precipitated using aqueous ammonium hexafluorophosphate. The precipitate was filtered and washed with H_2O and diethyl ether to yield a dark red powder (0.29 g, 78%). The ethyl ester groups of **$[RuP]_n$** were hydrolyzed by reaction with excess TMS-Br in MeOH to produce the oligomer with phosphonate anchor groups in the same manner as the monomer dye.[38]

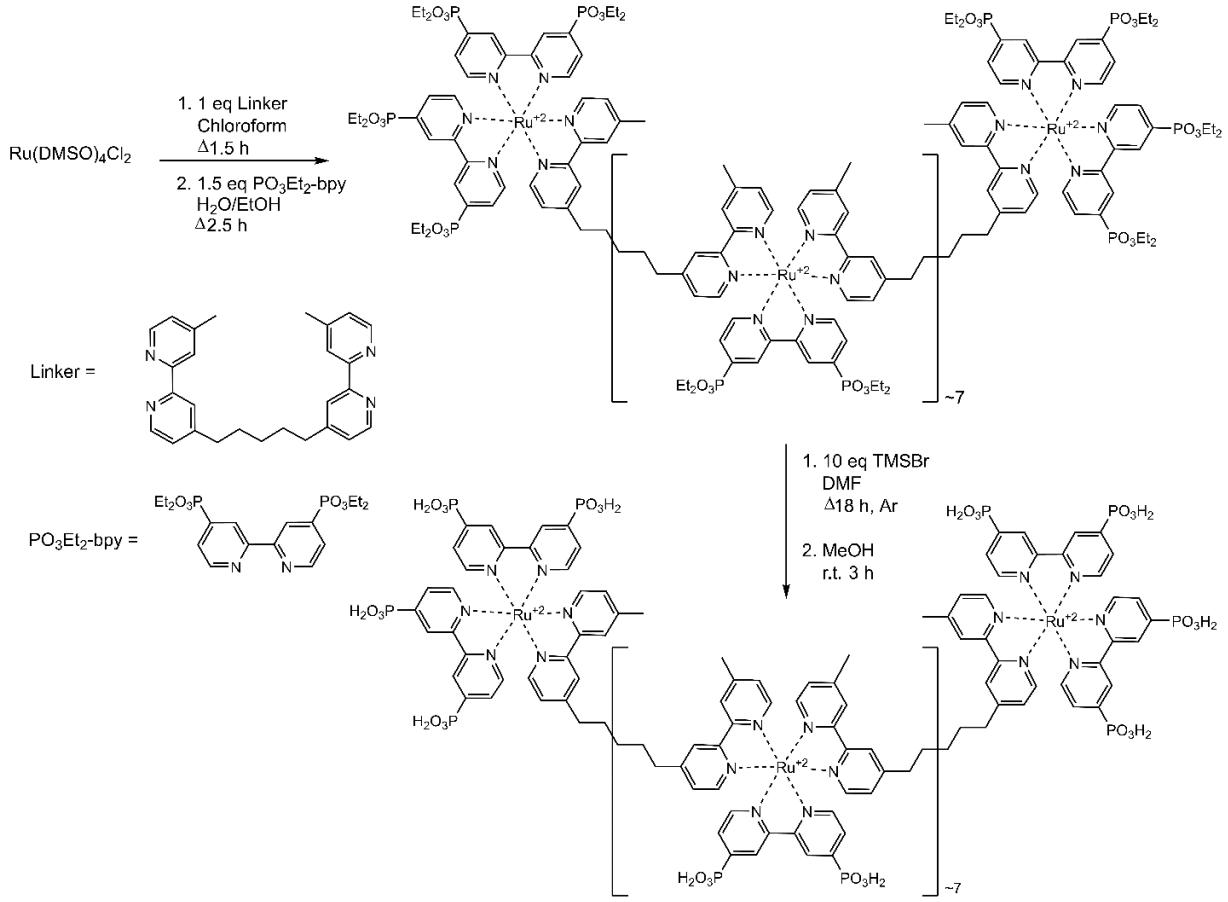

Figure 5. Synthetic scheme for $[RuP]_n$. First the oligomer is prepared from the ruthenium precursor and linker, then chain growth is capped using the $(4,4\text{-}PO_3Et_2)_2$bpy anchor group. Finally, anchor groups are formed by hydrolysis.

The degree of polymerization was determined using ^{1}H NMR spectroscopy analysis of end groups as performed in literature.[15] In the NMR spectrum of **$[RuP]_n$**, it is assumed that the end groups contained two phosphonated-2,2-bipyridine units and the interior Ru^{2+} centers had one. The degree of polymerization can then be calculated from the ratio between the average peak areas for the 1,5-bis(4-methyl-2,2-bipyridyl-4-yl)pentane units and phosphonated-2,2-bipyridine units, indicated in Figure 6. By this method, the average **$[RuP]_n$** molecule was determined to have about 7 metal centers.

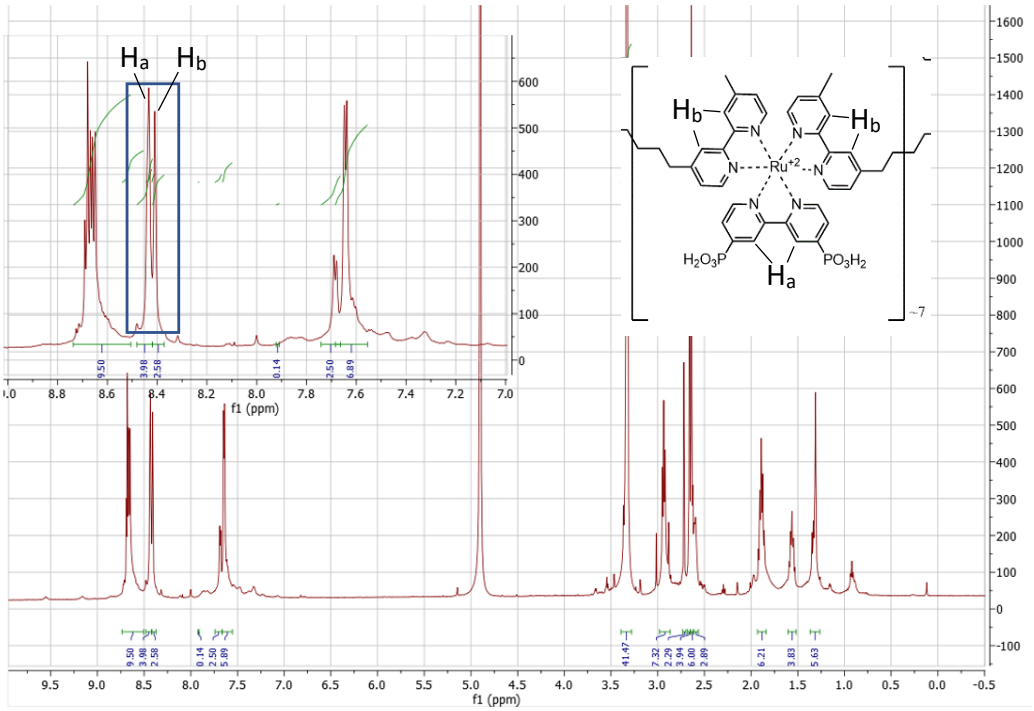

Figure 6. ^{1}H NMR Spectrum of $[RuP]_n$. The ratio between the two peaks within the boxed area is used to determine chain length. The downfield peak represents the anchor group due to electron withdrawal from the phosphonate. Peaks are labeled to their corresponding proton on the oligomer structure.

1.2.1 Gel Permeation Chromatography

Gel permeation chromatography (GPC) was performed on the ethyl-ester protected oligomer **$[RuP\text{-}Et]_n$** to determine the distribution of chain lengths. The sample was run in chloroform solution with molecular weights and dispersity measured using a Shimadzu pump (Shimadzu corporation), coupled with Shimadzu UV and RI detectors, controlled by an EZStart program, calibrated against polystyrene standards. The column and guard column utilized were pre-packed from American Polymer Standards in chloroform (AM GPC Gel, 10 μm pre-column, attached to 10 μm 500 Å, and linear mixed bed columns in $CHCl_3$; American Polymer Standards, Mentor, OH) and the column temperature was maintained at 40 ˚C. All samples were measured

with a mobile phase consisting of chloroform (Sigma-Aldrich, HPLC grade, containing amylene as a stabilizer). The injection volume was 10 µL and the flow rate was 1 mL min^{-1}.

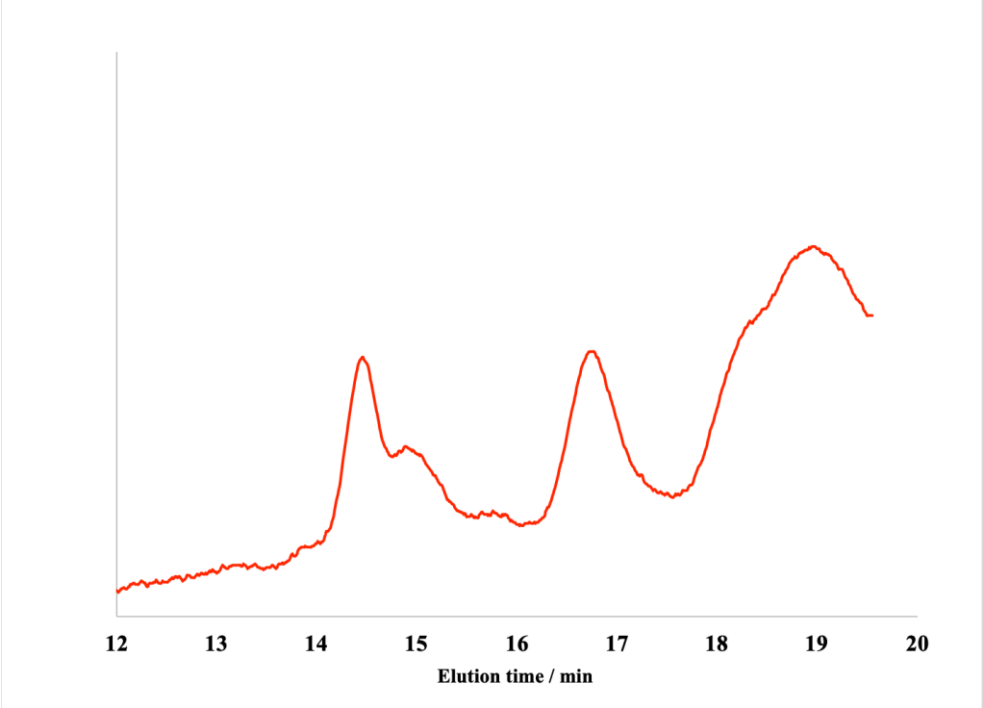

Figure 7. Gel permeation chromatography trace of oligomeric ethyl-ester precursor ([RuP-Et]$_n$)

Table 1. Gel permeation chromatography peak data for ([RuP-Et]$_n$)

Peak#	M_n (g/mol)	M_w (g/mol)	Dispersity (M_w/M_n)	n (Approx.)	%
Total	3400	12100	3.48	4-14	100.00
1	34400	35000	1.01	41	24.8
2	19300	19450	1.00	23	2.7
3	10800	10800	1.00	13	1.2
4	5600	5700	1.01	7	41.3
5	2300	2300	1.00	3	6.5
6	1270	1300	1.02	2	23.4

There were six distinct peaks in the GPC trace ranging from Mn = 1270 to Mn = 34400. The dispersity ($Đ_M$) of the entire sample was 3.48; however, if we consider only the oligomers

ranging up to 10 units long and comprising the majority of the sample, Đ = 1.56. Each peak is likely a combination of similar chain lengths that elute from the column together, owing to columns that are packed with crosslinked poly(styrene) beads specializing in separations of up to 1,000,000 g/mol. It is likely that all chain lengths of the oligomer exist in the sample and that the distinct peaks observed are a mixture of similar lengths that elute at similar times. For example, the heptamer peak is likely composed of chain lengths ranging from 5 to 9 units that elute at similar times. These results indicate the solution contains a broad distribution of chain lengths.

Considering the entire sample volume and oligomers detected by GPC, the overall dispersity was large; however, all constituent peaks comprised a narrow dispersity. Discrete signals corresponding to dimers and trimers represented 23.4% and 6.5% of the sample, respectively, while a heptamer peak could be observed that constitutes 41.3% of the sample. Intermediate length oligomers ($10{,}000 < M_n < 20000$) comprise approximately 3.9% of the sample. The longer chains ($M_n > 30000$), which comprise the remaining 24.8% of the sample, are unlikely to penetrate into the electrode pore network. Taking into account the spread of oligomers ranging from 2-10 units long in structure, the sample dispersity is 1.56, akin to what might be expected from a supramolecular polymerization that is likely both concentration and solubility limited.

1.3 Materials and Methods

1.3.1 Electrode Preparation

All electrodes were prepared on 18 Ω/cm^2 fluorine-doped tin oxide-coated glass (FTO-glass, Hartford Glass Company). A colloidal suspension of anatase TiO_2, prepared as previously described in literature,[16,41] was deposited onto the FTO-glass via the doctor blade method to form a 1 cm^2 area. Layers of transparent tape were used to control the thickness of the suspension that was applied to the electrodes. The resulting films were sintered at 300 °C for 20 min, 350 °C for 10 min, and 500 °C for 30 min. For one and two pieces of tape the thickness of the films was measured to be approximately 3 μm and 6 μm, respectively, by profilometry (Tencor P16+).

Electrodes were sensitized by soaking in 2 mL of 100 μM of sensitizer (**RuP** or **[RuP]$_n$**) in ethanol overnight at room temperature in the dark, then rinsed with ethanol and dried under a stream of N_2. Following dye deposition, electrodes were kept in the dark until use. Insulated silver-plated copper wire was attached to the electrode using silver paste (DuPont CP4922N-100), and contacts were protected using white epoxy (Loctite 1C Hysol). Absorption spectra of the electrodes were collected in ethanol solutions.

1.3.2 Emission Measurements

Steady-state emission data were collected at room temperature on a custom-built fluorimeter. For emission experiments, samples were excited using a light output from a housed 450 W Xe lamp. Sensitizer solutions were freshly prepared in ethanol at 100 μM concentration, added to quartz cuvettes, and degassed with nitrogen for 20 min. Emission studies conducted on sensitized electrodes were performed in argon-purged acetate buffer (pH = 4.8).

1.3.3 Photostability

The long-term adhesion of the sensitizer molecules was evaluated using a technique developed by Meyer and coworkers.[17] Briefly, the electrode was subjected to constant irradiation under open-circuit conditions in phosphonate buffer solution (pH = 7.8). The light from a high-power blue LED (455 nm, fwhm 30 nm, 475 mW/cm^2, Thorlabs, Inc., M455L2) powered by a T-Cube LED driver (Thorlabs, Inc., LEDD1B) was directed onto the sensitized electrodes placed at 45° in a standard 10 mm path length cuvette containing 5 mL of the solutions of interest. The incident light intensity was measured using a thermopile detector (Newport Corp 1918-C meter and 818P-020-12 detector). The absorbance of the electrodes was measured to determine the amount of dye still attached every 5 minutes over the first hour and every 15 minutes throughout the remainder of the experiment. The electrodes were rinsed with water between each measurement.

1.3.4 Cross-Surface Hole Transfer

All photoelectrochemical measurements were carried out using a Metrohm Autolab potentiostat (PGSTAT128N) in a three-electrode electrochemical cell using a Pt wire as the counter electrode and an Ag/AgCl (3 M NaCl) electrode as the reference electrode. Absorption spectra were recorded on a Cary 6000i UV-Vis spectrophotometer. Following the method of Hanson et. al.,[16,17] the cross-surface electron diffusion constant (D_{app}) was measured in 0.1 M $HClO_{4(aq)}$ by applying a potential of 2.0 V vs Ag/AgCl (3.5 M NaCl) for 5 min, then 0.0 V for an additional 5 min. D_{app} was calculated by monitoring the change in absorbance at 450 nm and then analyzing the data according to Equation 1-5:

$$\Delta A = \frac{2A_{max}D_{app}^{1/2}t^{1/2}}{d\pi^{1/2}} \quad (1\text{-}5)$$

Here ΔA is the change in absorbance (A_{max} - A(t)), A_{max} is the initial absorbance of the fully reduced film, t is the time in seconds, and d is the thickness of the film (6 μm). D_{app} was determined by fitting the change in absorbance over the linear portion of the experimental data.

1.4 Results and Discussion

1.4.1 Emission of Dye Aggregates

Aggregation of dye molecules on the electrode surface is a concern when constructing dye-sensitized electrodes. Molecules not directly adhered to TiO_2 through phosphonate anchor groups have lowered injection yields which leads to decreased efficiency of the photoelectrochemical cell.[42,43] Without an injection route to quench excited state dye molecules, the aggregates strongly luminesce. To ensure that electrodes were absent of dye aggregates, steady-state luminescence emission spectra was used to analyze the emission intensity of dye samples adhered to TiO_2 electrodes compared to dye samples in solution. Results are shown in Figure 8.

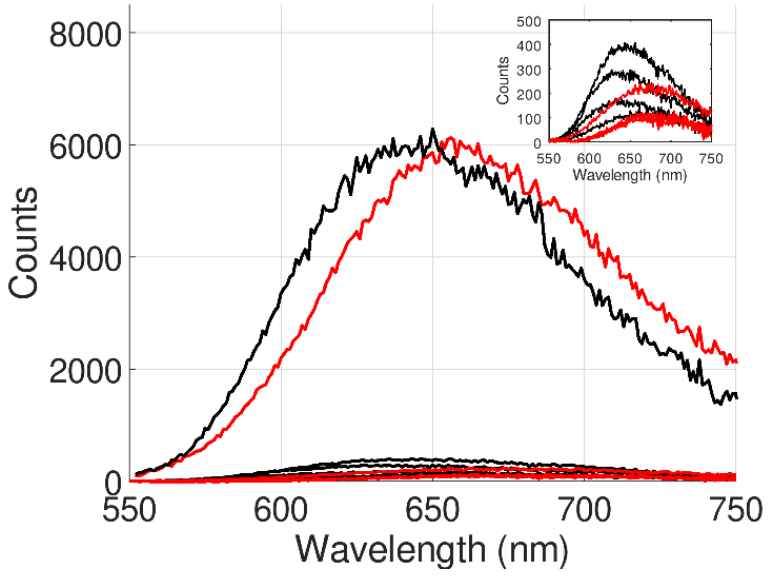

Figure 8. Steady state emission spectra of RuP (black) and $[RuP]_n$ (red) on electrodes (emission maxima ~200-400 cts) versus dye in solution (maximum ~6000 cts). Inset displays magnified spectra for dyes deposited onto electrodes.

When $Ru(bpy)_3$ derivatives are covalently anchored to semiconducting TiO_2, the excited state is rapidly quenched through electron injection into the conduction band.[44] Both sensitizers

RuP and **[RuP]$_n$** displayed weak luminescence when adhered to TiO_2 electrodes. Sensitizers dissolved in solution strongly luminesce, since there is no route to quench excited state dye molecules. The order of magnitude decrease in luminescence for the adsorbed dye molecules indicates that the electrode preparation methods result in the majority of dye complexes being directly attached to the TiO_2 surface by phosphonate anchor groups. Electrodes with dye aggregation would strongly luminesce as if the sensitizer molecules were in solution.

1.4.2 Photostability of Sensitizers

As previously discussed, dye desorption from the electrode surface is a major cause of inefficiency in WS-DSPECs. The results of constant dye irradiation under open-circuit conditions for 3h in phosphate buffer pH = 7.8 are displayed in Figure 9. The inset shows absorbance versus time at the maximum absorbance value of 450 nm. Phosphate buffer was used since the highest efficiency $Ru(bpy)_3$ cells have been reported in similar pH phosphate buffer solutions.[45] We observed that the absorbance of monomer-sensitized electrodes rapidly decreased due to dye desorption from the electrode, ultimately reaching the baseline absorbance of the TiO_2 after 3h. The ~60% drop in absorbance for **RuP** is consistent with observations from other groups working with monomeric, phosphonate anchored $Ru(bpy)_3$ dye complexes.[17,46] Under identical conditions, the oligomer-sensitized electrodes exhibit a 15% drop in absorbance over the first 30 min of irradiation but then display stable absorbance for the remainder of the experiment.

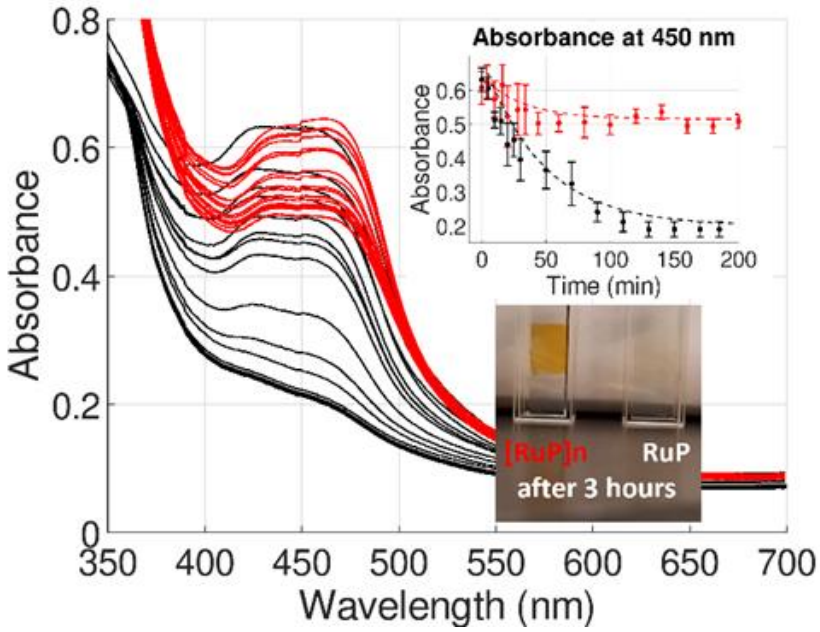

Figure 9. Absorbance of RuP (black) and $[RuP]_n$ (red) electrodes during the photostability experiment. Inset shows decay at peak absorbance wavelength. Photo shows visible dye saturation on electrodes after completion of the experiment.

The oligomer performs significantly better in stability studies than conventional monomeric $Ru(bpy)_3$ complexes. **$[RuP]_n$** experiences a smaller decay in absorbance at 450 nm than **RuP** and exhibits a steady absorbance of 0.51. In pH 4.8 buffer solution, the oligomer also remained adhered to electrodes longer than monomer during the photostability experiment. The high steady absorbance for **$[RuP]_n$** is profoundly significant in studying WS-DSPECs. The synthesis of an oligomeric phosphonated $Ru(bpy)_3$ dye complex which is stable at high pH allows for the electrochemical study of WS-DSPECs at a much broader pH range, including at pH 6.8 where the highest efficiency cells have been reported.[45] The results of this photostability study for our oligomer demonstrate such viability under a broader pH range. Studies of electrochemical cell performance as a function of pH that were previously inaccessible due to rapid monomer desorption could now be possible using **$[RuP]_n$**.

1.4.3 Cross-Surface Hole Transfer

In WS-DSPECs, hole diffusion between oxidized and reduced sensitizer molecules is an important process to connect the photoinduced charge transfer and catalytic water oxidation steps. The apparent cross-surface hole transfer diffusion coefficient, D_{app} was measured for TiO_2 films sensitized with ethanol solutions of **RuP** and **[RuP]$_n$**. Spectroelectrochemical absorbance data for a typical monomer and oligomer-sensitized electrode are shown in Figure 10.

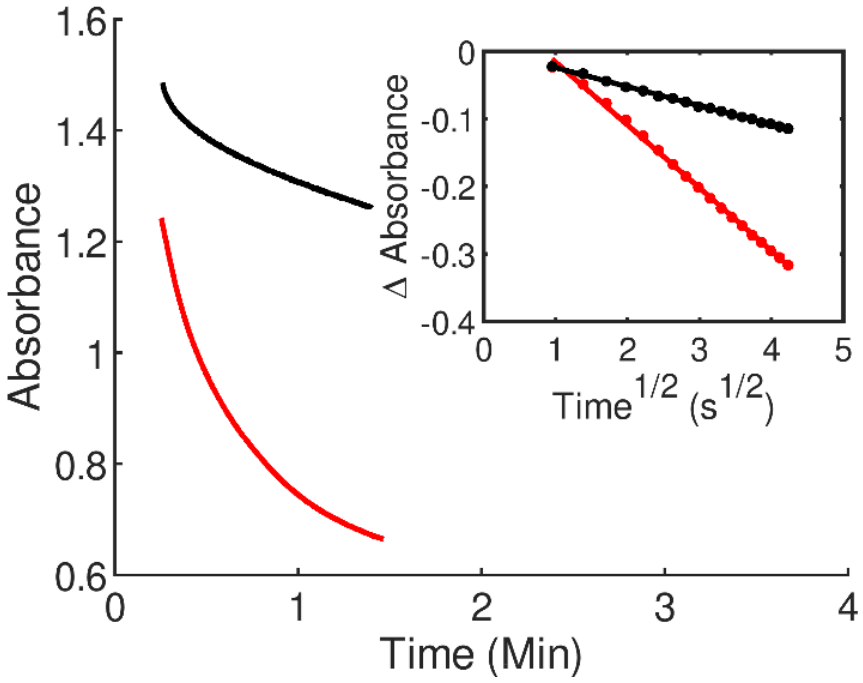

Figure 10. Representative set of absorbance versus time data during the cross-surface hole transfer study used to calculate D_{app} values for RuP (black) and [RuP]$_n$ (red) electrodes. The inset fits the data to Equation 1-5 over the linear region for the drop in absorbance.

Before the experiment begins, the dye absorbs incident photons at a maximum value and injects electrons into TiO_2. The photoanode is absent of an OER catalyst, so the majority of oxidized dye molecules are quenched by recombination and continue to absorb photons; a miniscule current of electrons flow to the platinum electrode. The intense 2.0 V overpotential prevents recombination; all electrons injected into TiO_2 travel through the potentiostat to the

cathode. The overpotential effectively oxidizes all illuminated dye molecules and prevents further light absorption, so a decrease in absorbance is realized. Since the incident photon beam path is small compared to the area of the photoanode, much of the dye is not illuminated and therefore not oxidized. These non-illuminated dye molecules can each transfer one electron to the illuminated area, where it will then be injected into TiO_2 and transferred to the cathode. Dye molecules further from the illuminated area can transfer an electron to an oxidized dye molecule, this "hole-hopping" continues until the entire electrode surface is oxidized and the absorbance reaches a minimum. The drop in absorbance is proportional to the rate of electron transport to the illuminated area which is comparable to hole transfer to a catalytic site in a WS-DSPEC.

Table 2. Cross-surface hole diffusion constants for synthesized sensitizers

Sensitizer	D_{app} (cm^2/s)
RuP	$1.79 \pm 0.58 * 10^{-10}$
$[RuP]_n$	$28.1 \pm 1.6 * 10^{-10}$

D_{app} was calculated as the slope of the fitted data for the linear region of the drop in absorbance and is recorded in Table 2. The monomer values (black lines in Figure 10) are in good agreement with literature values for monomer deposited from ethanol.[16] By covalently linking the oligomer units together the hole diffusion constant is increased by an order of magnitude relative to the monomer. It should be noted that D_{app} is an apparent measurement for the entire photoanode surface, meaning it is an averaged value of all possible hole transfer mechanisms. It is possible that hole transfer between metal centers on the oligomer is fast relative to D_{app}, which is likely limited by hole transfer between chains adsorbed on the electrode surface.

It has also been shown that an order of magnitude increase in D_{app} can be obtained by depositing the monomer from aqueous 0.1 M $HClO_4$,[16,17] compared to deposition from ethanol. However, the Mallouk group has previously shown that acidic depositions negatively affect the

photocurrent and overall performance of the electrodes.[16,47] The oligomer is not soluble in aqueous $HClO_4$ solutions, so it was not possible to compare the monomer and oligomer from acidic deposition solutions. Nevertheless, the oligomer displays significant improvement over the monomer, while avoiding the complications of acidic deposition solutions.

1.5 Conclusions

Photostability of sensitizers and cross-surface hole diffusion on the electrode surface are two properties that have received recent attention as key limiting factors in the efficiency of WS-DSPECs. The newly synthesized oligomeric dye **[RuP]$_n$** has dramatically improved electrode adhesion at pH 4.8 and pH 7.8. Long-term stability of the **[RuP]$_n$** was also observed at higher pHs traditionally incompatible with monomeric dyes. This finding allowed for the performance of previously inaccessible experiments, such as the measurement of charge recombination from TiO_2 to oxidized dye molecules by intensity-modulated photovoltage spectroscopy as a function of pH.[1] The apparent hole diffusion constant of **[RuP]$_n$** was an order of magnitude higher than the monomeric **RuP**, indicating the oligomer's effectiveness in enhancing cross-surface transport of oxidizing equivalents to OER catalytic sites. These results demonstrate that oligomeric dyes are an effective strategy in designing high-stability chromophores for WS-DSPECs.

An essential future direction for experimentation is to compare **RuP** and **[RuP]$_n$** as sensitizers in working WS-DSPECs. The experiments described in this report measured certain metrics such as photostability and cross-surface hole diffusion which indicate that the oligomer would perform better than the monomer in a water-splitting system. Incorporation of **[RuP]$_n$** into a WS-DSPEC would provide more thorough metrics by which to define the sensitizer such as solar-to-hydrogen efficiency and allow for direct comparison between **[RuP]$_n$** and other studied sensitizers. Additionally, the synthesis of **[RuP]$_n$** should be optimized or a separation process established to ensure a smaller dispersity of chain lengths. Our findings are currently associated with the heptamer as it represents the plurality of active dye molecules on our electrodes; however, isolating and comparing sensitizers of various chain sizes could confirm this hypothesis.

Chapter 2

Liquid Imidazolium Zwitterions to Improve Conductivity of Lithium Ion Battery Polyelectrolytes

2.1 Introduction

2.1.1 Solid-State Polyelectrolytes in Lithium Ion Batteries

The development of lithium ion batteries (LIBs) has drastically impacted modern technology as recognized by the 2019 Nobel Prize in Chemistry.[48] Commercially available LIBs are optimized with large gravimetric energy densities and minimal charge loss after repeated charging cycles.[49] A significant disadvantage of contemporary LIBs is the use of organic electrolytes such as ethylene carbonate, diethylene carbonate, or dimethyl carbonate to ensure high lithium ion conductivity and rapid discharging. These solvents are highly flammable and damaged batteries are known to explode or cause serious fires; therefore, LIBs must be protected with a durable, bulky encasing. Solid-state polymeric electrolytes, polymers with ions covalently anchored to the backbone, are a rapidly developing technology which could eliminate the use of dangerous organic electrolytes in LIBs. Solid-state polyelectrolytes can be designed to have large energy densities, low flammability, chemical stability, and widely tunable physical properties.[50] They could eliminate the need for a protective encasing, both increasing the gravimetric energy density of LIBs while enhancing safety. Additionally, the mechanical properties of solid-state polymers could promote the development of flexible LIBs as well as other electrochemical membranes such as polymeric actuators.[51]

Unfortunately, one significant drawback of solid-state polymer electrolytes is poor ionic conductivity since intermolecular forces inhibit dissociation of ions from the polymer backbone.[52]

Lithium polymer batteries, common in household electronics, already use a polymer electrolyte; however, the polymer must be swollen with volatile solvent to sufficiently increase the ionic conductivity.[53] One proposed solution to improving ionic conductivity without organic solvents is the introduction of ionic liquids into polymer electrolytes. Ionic liquids are composed entirely of cations and anions; they can act as both a charge carrier and a plasticizer in polymer electrolyte systems.[54,55] While useful, addition of ionic liquids in significant quantities often sacrifices desired mechanical properties in polyelectrolytes. Moreover, the mobility of ionic liquids in an electric field will compete with lithium ion transport to lower the overall lithium conductivity and charge density in battery systems,[56] thus an alternative solution to the problem of low ionic conductivity in solid-state polyelectrolytes is necessary.

2.1.2 The Zwitterion Effect in Conductive Materials

Zwitterions are small molecules that simultaneously possess both cationic and anionic functionality, resulting in useful material properties. Arguably the most widespread zwitterions are amino acids, which under moderate pH conditions possess both a carboxylate and ammonium functional group. Researchers have found use for zwitterions as mediators in organic synthesis;[57] however, the majority of applications exist in the field of biochemistry and biochemical materials. Many zwitterions are extremely hydrophilic and repel proteins resulting in their use as antifouling coatings.[58] Zwitterionic monomers are frequently polymerized to create more tenacious coatings which are resistant to bacterial adhesion[59] and nonspecific protein adsorption.[60] These zwitterionic polymers are applied in medical fields as protective coatings on biomedical implants, drug delivery systems, and blood contacted sensors.[59]

More recently have zwitterions been applied in electrochemical membrane applications. Based on previous success using imidazolium-based ionic liquids to increase conductivity in lithium ion battery polymer electrolytes,[54] Forsyth and co-workers observed that imidazolium zwitterions such as 1-butylimidazolium-3-(n-butanesulfonate) (**BImBS**) at 9 wt% could yield up to a sevenfold enhancement in conductivity.[56] It was confirmed by NMR spectroscopy that conductivity was a result of increased lithium ion mobility; however, the cause of this "zwitterion effect" is still not well understood. It is believed that a zwitterion's static dielectric constant is related to its ability to improve ionic conductivity; 1-methylimidazolium-3-(n-propanesulfonate) (**MImPS**) has an exceptionally high static dielectric constant, ε_s = 76, and improves ionic conductivity 300 fold in polymer actuator systems.[51] This extreme enhancement of ionic conductivity indicates that zwitterions could be added to polyelectrolytes in much smaller ratios than ionic liquids. Additionally, use of zwitterions to increase conductivity in battery membranes yields higher lithium ion transport metrics than addition of ionic liquids since introduction a single dipolar molecule to a system avoids complications that arise when adding free ions such as competition in ionic migration.[56]

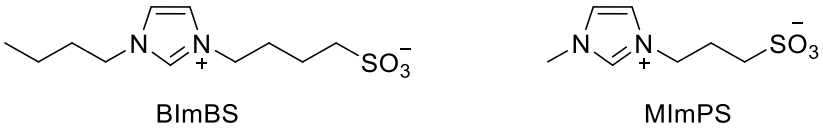

Figure 11. Structures of two imidazolium sulfonate zwitterions used to increase the ionic conductivity of polymer systems.

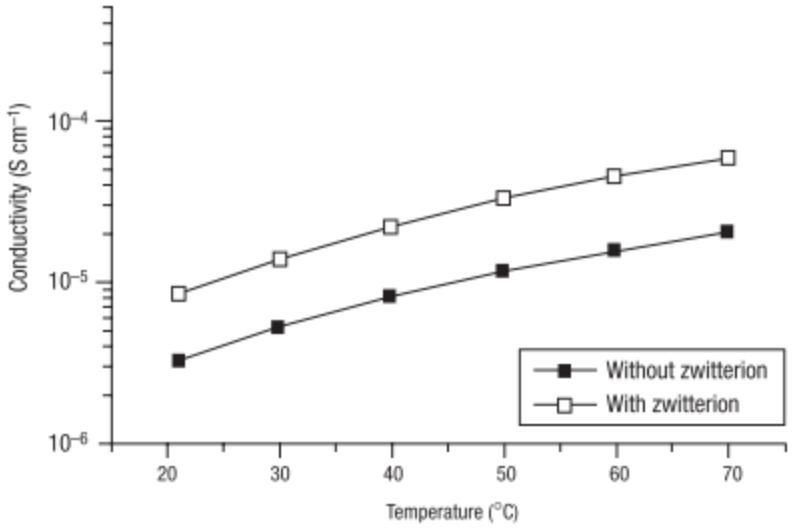

Figure 12. BImBS zwitterion at 9 wt% increases the conductivity of 10:90 P(MALi-c-DMAA) in PEG solution (Reproduced from Ref. [56])

2.1.3 Advantages of Low-Melting Temperature Zwitterions

Many zwitterions have higher melting points than corresponding ionic liquids since the tethering of ions decreases the degree of molecular motional freedom.[61] For instance, **BImBS** has a melting temperature of 152 °C and generally can only be present in less than 10 weight percent in polyelectrolyte systems before precipitating from solution.[56] It is important for a polyelectrolyte system to have a glass transition temperature, T_g, lower than the intended temperature of use in order to achieve the highest possible ionic conductivities. A material's T_g marks the thermal range where a phase transition occurs from an amorphous, brittle, glassy state to a rubbery, viscous state as the temperature is increased. In general, ionic conductivity is inversely proportional to T_g for PIL systems since the increased flexibility of polymer chains above the glass transition supports more effective ion transport.[62] Glass transition for a system of multiple components generally follows the Fox equation,

$$\frac{1}{T_g} = \frac{w_1}{T_{g,1}} + \frac{w_2}{T_{g,2}} \qquad (2\text{-}1)$$

where the predicted T_g is determined by the weight fraction ($w_{1,2}$) and glass transition ($Tg_{1,2}$) of each of the components; therefore, introduction of a high T_g zwitterion increases the overall T_g for the conductive polymer system.

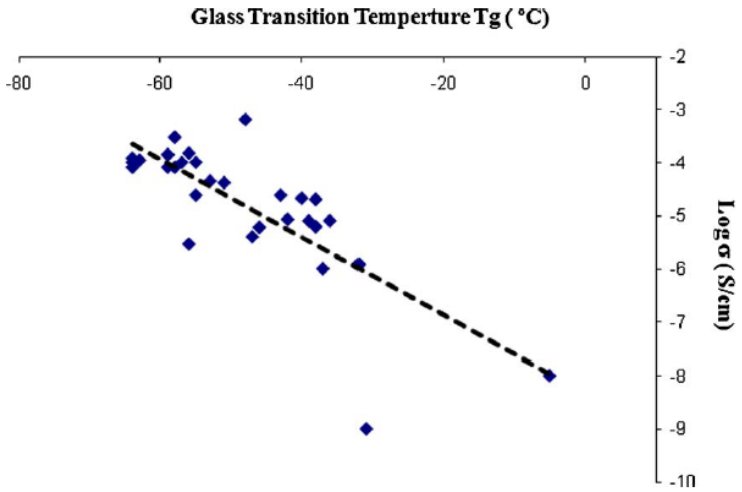

Figure 13. Relationship of T_g and ionic conductivity for a selection of PILs reported in literature (Reproduced from Ref. [62])

Zwitterions which are liquid at room temperature should more significantly improve polyelectrolyte conductivity at appropriate conditions for lithium ion battery usage. Rikukawa and co-workers have developed a class of low-melting temperature zwitterions similar to **BImPS** (the propyl sultone analogue of **BImBS**) by incorporating two oxyethylene units in place of the butyl chain to achieve glass transition temperatures as low as -32 °C.[63] In these **OE_2ImPS** zwitterions, the bulky oxyethylene sidechain greatly enhances the motional freedom and depresses the molecular interactions between zwitterions, lowering T_g and increasing ionic conductivity in $LiN(Tf)_2$ solution. The oxyethylene imidazole unit (**OE_2Im**), provides a useful starting point for the synthesis of other sulfonate zwitterions as well as those with alternative anions such as carboxylate or phosphate. Investigation of this class of **OE_2Im** zwitterions may be particularly

useful in the development of polyelectrolyte systems with increased ionic conductivities at room temperature.

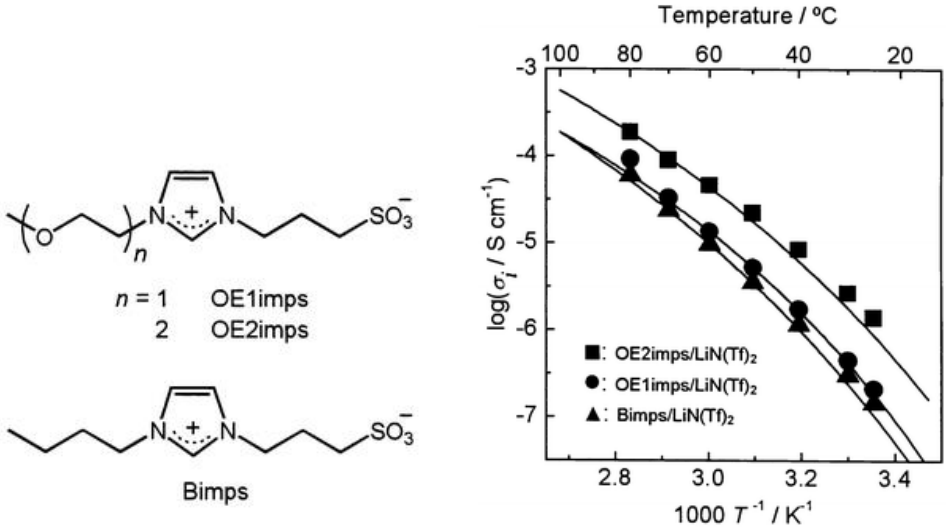

Figure 14. OE_2Im Zwitterions and comparison of ionic conductivity in 50 mol% $LiN(Tf_2)$ solutions (Reproduced from Ref. [63])

Another advantage of lowered T_g is the ability to quantify the zwitterion's static dielectric constant at a wider range of temperatures. Dielectric relaxation cannot be effectively measured when a zwitterion is in a glassy state (below T_g); a solution must be prepared with the zwitterion mixed into a solvent or ionic liquid and the dielectric constant estimated by extrapolation. For this reason, dielectric properties are typically seldom reported for zwitterions at low temperatures. Direct measurement of dielectric relaxation at room temperature would be a significant improvement in quantitative comparison of a zwitterion's ability to increase ionic conductivity.

2.1.4 Dielectric Relaxation Spectroscopy

A brief description of dielectric relaxation spectroscopy (DRS) is subsequently provided. For a more comprehensive analysis of the theory and practice relating to DRS, consult Kremer and

Schonhals' *Broadband Dielectric Spectroscopy*.[64] DRS analyzes the behavior of charged species in a small, alternating electric field. Small molecule dipoles freely rotate to align with the field; however, at high frequencies and low temperatures they become frozen, unable to overcome the steric barrier required for rotation. This transition between the mobile and frozen state is referred to as the relaxation time, τ.

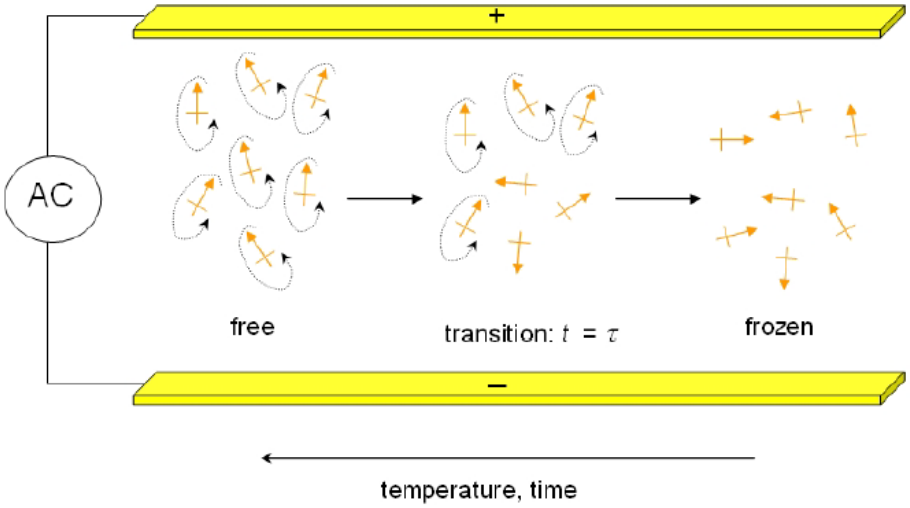

Figure 15. Dipole rotation between two charged electrodes. As a function of temperature and frequency, the dipoles transition from freely rotation to being frozen at the relaxation time, τ. (Reproduced from Ref. [65])

A dielectric relaxation can be observed by measuring the dielectric constant, also referred to as the dielectric permittivity, with respect to the oscillation frequency of the applied electric field. The dielectric constant is a function of both frequency and temperature, related through the concept of time-temperature superposition. It is a measure of a material's polarizability and ability to store electric charge. The complex dielectric constant ε is described as the sum of the real constant ε', representing charge stored in the material, and the imaginary constant ε'', representing dissipated charge.

$$\varepsilon(\omega) = \varepsilon'(\omega) + i\varepsilon''(\omega) \qquad (2\text{-}1)$$

At temperatures above and frequencies below the dielectric relaxation, the real part of the dielectric constant ε' is larger than ε'' since dipoles are able to respond to the applied field. The opposite occurs at temperatures below and frequencies above the relaxation since the dipoles become frozen. At constant temperature, ε' increases with decreasing frequency as dipoles unfreeze. Once all dipoles can freely rotate, a plateau is observed and ε' becomes independent of frequency. The static dielectric constant, ε_s is described as this plateau in ε', depicted in Figure 16. The metric is useful when directly comparing the capacity of zwitterions to increase ionic conductivity, since it is only a function of temperature. Zwitterions with large ε_s are highly polarizable and should be extremely effective in increasing ion mobility in polyelectrolytes.

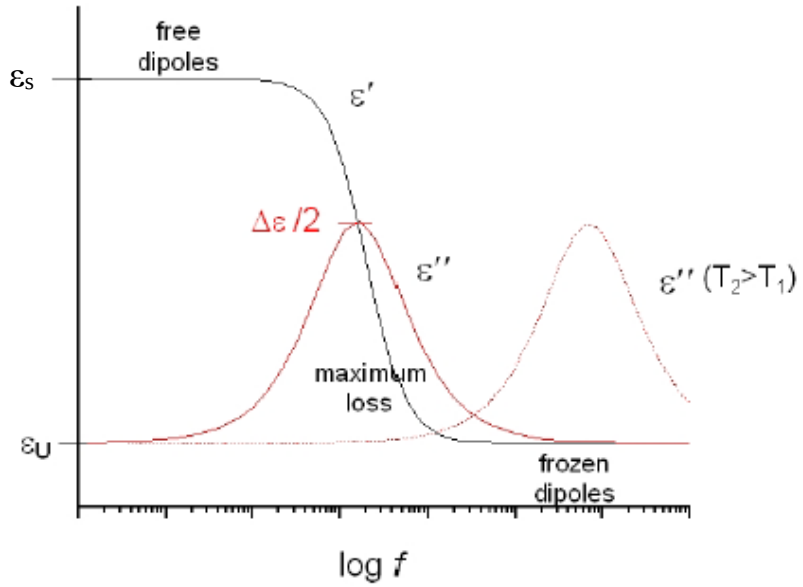

Figure 16. Graphical relationship between, ε', and ε" as a function of frequency. The static dielectric constant is denoted by ε_s. As temperature is increased, maximum loss occurs at higher frequency. (Reproduced from Ref. [65])

2.1.5 Summary of Project

The primary goal of this project is to synthesize and investigate the previously unreported static dielectric constants for the **OE$_2$Im** class of zwitterion to quantitatively determine their ability to increase ionic conductivity. The synthetic route to obtain **OE$_2$ImPS** and **OE$_2$ImBS** is adapted from Yoshizawa-Fujita et al.[63] **OE$_2$ImBS** is a newly reported zwitterion, synthesized by the ring opening of butyl sultone with **OE$_2$Im**. Synthesis of two otherwise equivalent zwitterions allows for the effect of distance between formal charges to be analyzed with respect to molecule's glass transition temperature and static dielectric constant.

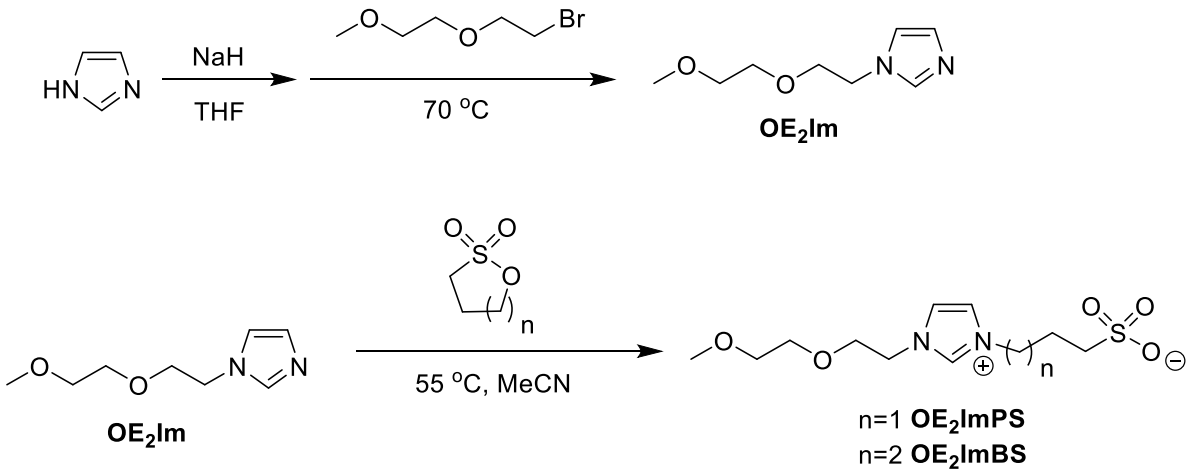

Figure 17. Scheme for the synthesis of OE$_2$Im type sulfonate zwitterions after Yoshizawa-Fujita et al.[63]

A second goal of this project is to synthesize an **OE$_2$Im** zwitterion functionalized with a phosphate anion, **OE$_2$Im(R-OP)**. The route towards **OE$_2$Im(R-OP)** was based on a procedure to synthesize zwitterionic monomers for polyzwitterions by Emrick and co-workers.[66] The phosphate anion is derived from 2-chloro-1,3,2-dioxaphospholane 2-oxide (**COP**). Advantages of the phosphate functionality include enhanced biological compatibility compared to sulfonate as well as a customizable alcohol R-group. The use of alcohols of various steric bulk could introduce

increased control of the glass transition temperature and lead to the synthesis of a large class of useful, novel **OE_2Im** phosphate zwitterions.

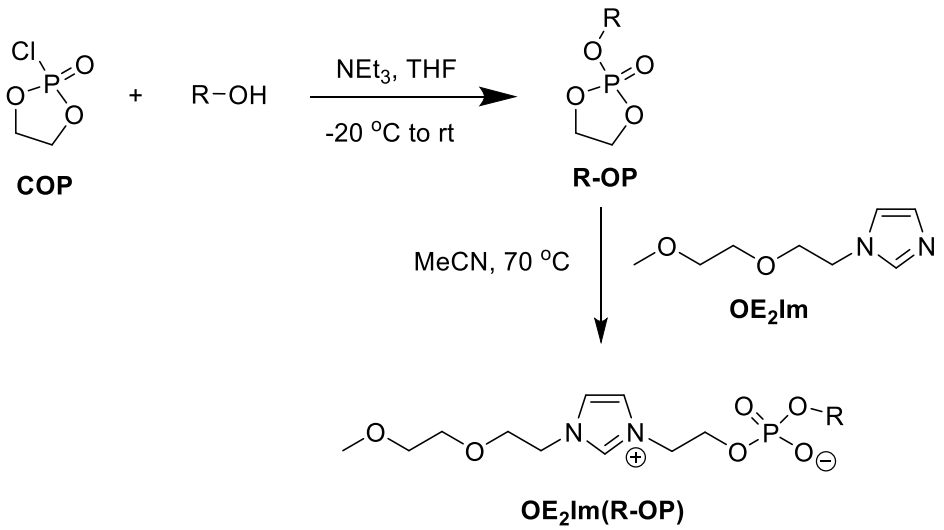

Figure 18. Proposed scheme for the synthesis of a phosphate functionalized OE_2Im zwitterion.

2.2 Analytical Methods

2.2.1 Differential Scanning Calorimetry

Glass transition temperatures (T_g) were determined using a TA Instruments Q2000 V24.11 Build 124 differential scanning calorimeter (DSC). Samples for DSC measurements were of mass 6-8 mg placed in aluminum hermetic pans, dried in a vacuum oven at 70 °C for 24h, and sealed by cold welding on a Tzero press. Samples were held at 125 °C for 5 minutes to ensure absence of water, then cooled to -75 °C at a rate of 10 °C/min and subsequently heated to 125 °C at 10 °C/min. T_g was obtained from the heating scan as the midpoint of the heat capacity transition.

2.2.2 Dielectric Relaxation Spectroscopy

Samples for DRS measurements were placed onto a brass electrode and dried in a vacuum oven at 70 °C for 12 h, after which a second brass electrode was placed on top of the sample. Silica spacers were used to control the sample thickness at 50 μm. A Novocontrol GmbH Concept 40 broadband dielectric spectrometer was used to measure the dielectric permittivity. Frequency sweeps were performed isothermally from 10 MHz to 0.1 Hz in the temperature range from 243 to 473 K. In order to minimize the amount of water in the samples and to avoid a change in water content during the experiment, the samples were initially held at 393 K for 45 min, and the measurements were performed during subsequent cooling under a flow of dry N_2.

2.3 Results and Discussion

2.3.1 Synthesis of Zwitterions

OE_2ImPS and **OE_2ImBS** were successfully synthesized and identified by ^1H NMR spectroscopy. The yield of **OE_2Im**, 56.9%, was much higher than recorded in literature (24.8%) which was attributed to increasing the reaction time for functionalization of the imidazole anion with 1-bromo-2-(2-methoxyethoxy)ethane under reflux conditions. **OE_2Im** conversion to the sulfonate zwitterions would be expected to be nearly stoichiometric; however, a yield of 73.6% and 77.8% for was achieved for **OE_2ImPS** and **OE_2ImBS**, respectively, indicating that the reaction did not proceed to completion. A longer reaction time or more concentrated reaction mixture may achieve higher yields.

A preliminary synthesis of the phosphate zwitterion was attempted using isopropyl alcohol as the R-group; thus, the target zwitterion will be referred to as **OE_2Im(iPr-OP)**. Isopropyl alcohol was used for these preliminary syntheses due to effective visualization of species during ^1H NMR spectroscopy; the presence of unexpected isopropyl heptets allows for straightforward identification of synthetic byproducts. The conversion of **COP** to **iPr-OP** was successful; however, it was difficult to purify the crude reaction mixture. A known impurity exists in the purchased **COP** reagent, 2-chloro-1,3,2-dioxaphospholane, which is identified on the NMR spectra. Previous syntheses performed in literature remove this impurity by distillation;[67,68] however, insufficient vacuum power prohibited us from replicating the technique. Normal phase chromatography was attempted; however, **iPr-OP** was not significantly moved by MeOH on a silica TLC plate. Reverse phase liquid chromatography would likely be an effective method to purify **iPr-OP**, but time and resource constraints did not allow for its exploration.

Unreacted triethylamine also remained as an impurity in the crude product. Cyclic ethylene phosphates undergo rapid hydrolysis under acidic conditions,[69] so an acid/base extraction could not be used to remove the excess triethylamine. After exposure to high temperatures in a vacuum oven, additional isopropyl peaks appear on the ^{1}H NMR spectrum, indicating that the triethylamine likely reacts with **iPr-OP** to form an unwanted zwitterion.

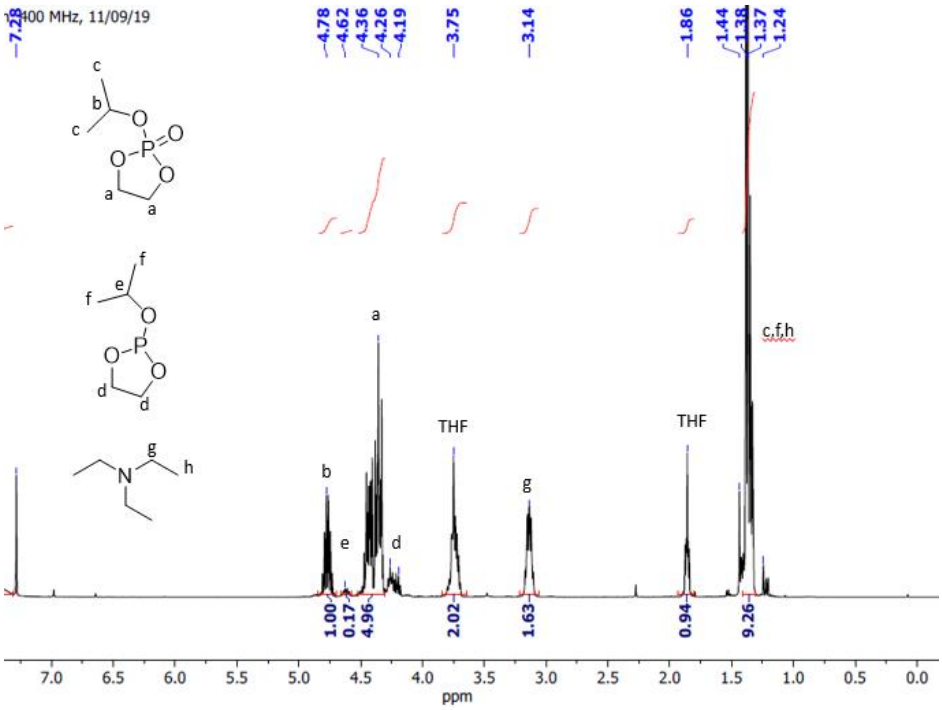

Figure 19. ^{1}H NMR of crude sample. 2-Chloro-1,3,2-dioxaphospholane is a known impurity in the purchased reagent.

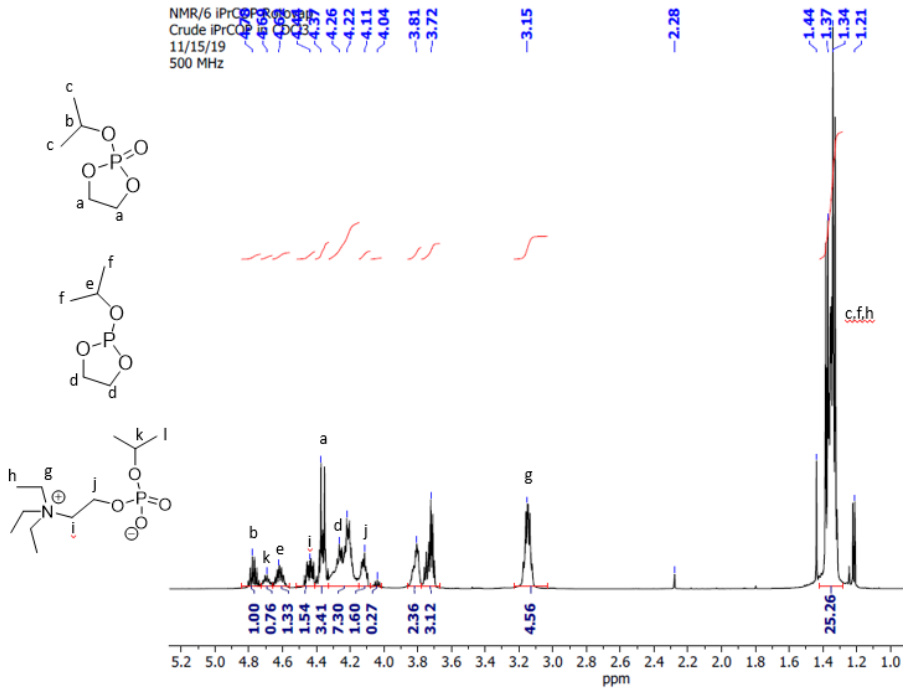

Figure 20. ^{1}H NMR of sample after heating to 70 °C at 100 mbar. Note the previously absent isopropyl heptet k indicating formation of a new species.

It was found that 1-methyl imidazole (pKa of conjugate acid = 7.06) could be substituted for the more basic triethylamine (pKa of conjugate acid = 10.75) with similar reaction yield at otherwise equivalent conditions. This technique bypasses the removal of the triethylamine at high temperature, since the unreacted 1-methyl imidazole can be used to functionalize **MIm(iPr-OP)**, a synthetic zwitterion analogue to **OE$_2$Im(iPr-OP).** At this stage in the synthesis, 1-methyl imidazole was used in place of **OE$_2$Im** due to affordability. Functionalization of the crude **iPr-OP** sample with 1-methylimidazole was attempted, anticipating that separation of the zwitterion from byproducts would be more straightforward; however, **MIm(iPr-OP)** ultimately could not be isolated. Thus, the synthesis and analysis of an **OE$_2$Im(R-OP)** zwitterion was not completed as of the submission of this report.

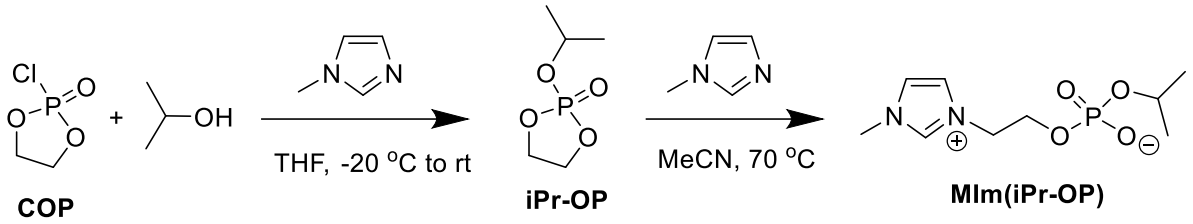

Figure 21. Attempted synthesis of MIm(iPr-OP) as a precursor to OE_2Im(iPr-OP).

While useful for synthetic study, it would not be recommended to use the expensive **OE_2Im** as a base since a majority of the reagent will be converted to the imidazolium salt. Trimethylamine was considered as a potential basic species with the advantage that it is gaseous at room temperature and unreacted reagent would be removed without external heating. Synthetic complications resulting from the use of gaseous reagents prevented the results of the study from being reported in this thesis.

2.3.2 Glass Transition Temperatures of OE_2Im Zwitterions

Differential scanning calorimetry (DSC) was performed on the synthesized zwitterions. DSC measures the heat flow into and out of a sample along a temperature range compared to a standard; it is a common method to determine the melting temperature, crystallization temperature, and the glass transition of materials, especially polymers. Phase transitions result in positive or negative peaks on the thermogram when excess heat is released or absorbed by the sample. It is often necessary to perform a full cycle of heating and cooling to erase the thermal history of a material to ensure accuracy when measuring the phase transitions. The DSC traces for the **OE_2Im** sulfonate zwitterions are displayed in Figure 22.

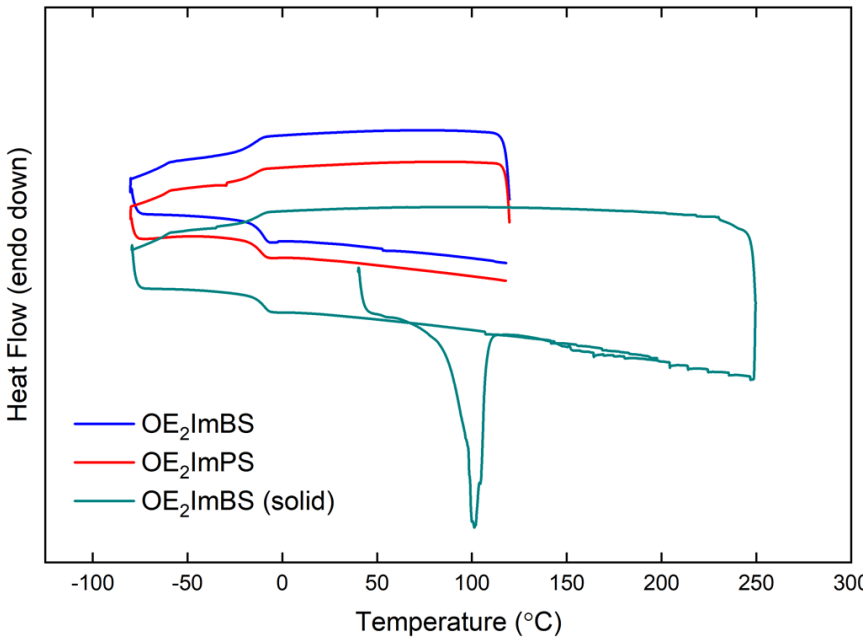

Figure 22. DSC trace for OE_2Im sulfonate species. A metastable phase for the OE_2ImBS was observed; after an initial heating cycle no further crystallization was observed.

Consistent with literature,[63] newly synthesized **OE_2ImPS** and **OE_2ImBS** displayed only a glass transition due to the bulky oxyethylene chain preventing crystallization. However, if allowed to sit for two weeks in a glovebox at room temperature, **OE_2ImBS** began to crystallize. DSC analysis of this crystalline sample showed a melting temperature during the first heating cycle; however, a crystallization peak was absent during cooling and the melting peak was absent during the second heating cycle. A metastable phase likely exists for the **OE_2ImBS** sample, indicating that the oxyethylene chain is not bulky enough to completely nullify the strong intermolecular forces between zwitterions. It is unclear why the **OE_2ImPS** sample does not exhibit a similar metastable crystallization; the phase transition may occur on a much longer timescale. The glass transition temperatures for the samples were reported at the midpoint of the endothermic glass transition and are recorded in Table 3.

Table 3. Glass transition temperatures for OE_2Im sulfonate zwitterions

Zwitterion	T_g (°C)
OE_2ImPS	-9.85
OE_2ImBS	-10.85

While the measured glass transition of **OE_2ImPS** is 20 °C higher than the value reported in literature;[63] the purity of our samples was confirmed by ^{1}H NMR spectroscopy so we believe the results to be genuine. **OE_2ImBS** was shown to have a slightly lower T_g than the propyl sultone analogue. This finding can be attributed to the increased flexibility of ions due to the longer spacing between cations and anions in **OE_2ImBS**; similar findings have been reported by Ohno and co-workers in the study of melting temperatures of zwitterions.[61] In general, increasing the distance between formal charges in zwitterions has been shown to lower the melting temperature and by extension the glass transition temperature.

2.3.3 Static Dielectric Constants of OE_2Im Zwitterions

As previously mentioned, dielectric relaxation spectroscopy (DRS) is a useful technique to determine the polarizability of the synthesized zwitterions, which is hypothesized to be related to their ability to increase ionic conductivity. DRS was performed on samples of pure **OE_2ImPS** and **OE_2ImBS** to determine the static dielectric constant ε_s. Temperature was held constant and electric field oscillation frequency varied to determine the values of ε'. A sample plot of ε' as a function of frequency at 25 °C is provided in Figure 23. Similar plots were constructed at each temperature tested between 0 °C to 150 °C.

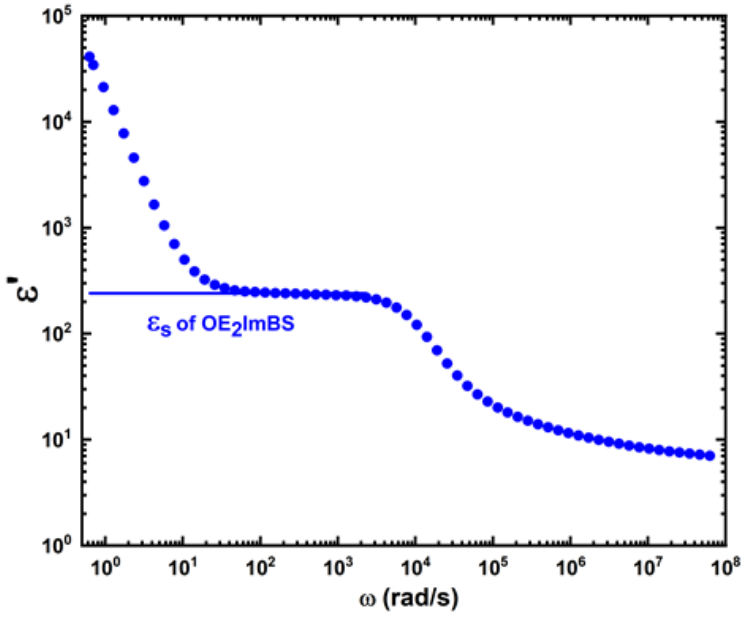

Figure 23. The static dielectric constant of OE_2ImBS was determined by measuring epsilon prime as a function of frequency at a constant temperature. The above data was collected at 25 °C.

An ideal relaxation plateau is observed in ε' for the synthesized zwitterions when frequency is varied at constant temperature. The dielectric constant at the plateau is referred to as the static dielectric constant ε_s. The observed increase in ε' after the relaxation is due to the electrode polarization effect from ions accumulating on the electrodes; the effect is common in DRS experimentation. A full list of $\varepsilon_s$values measured at 10 °C intervals from 0 °C to 150 °C is included in Table 4 and depicted graphically from 10 °C to 150 °C in Figure 24.

Table 4. Static dielectric constants for OE_2Im sulfonate zwitterions

Temperature (°C)	1000/T (K^{-1})	OE_2ImPS	OE_2ImBS
150	2.363	148.5	177.8
140	2.420	152.8	182.9
130	2.480	156.0	187.6
120	2.544	161.9	192.7
110	2.610	166.2	197.7
100	2.680	170.7	203.7
90	2.754	174.7	209.5
80	2.832	179.7	215.4
70	2.914	184.5	220.6
60	3.002	188.4	227.2
50	3.095	193.2	233.2
40	3.193	197.6	242.5
30	3.299	201.2	249.8
20	3.411	204.8	259.1
10	3.532	207.6	268.0
0	3.661	-	275.0

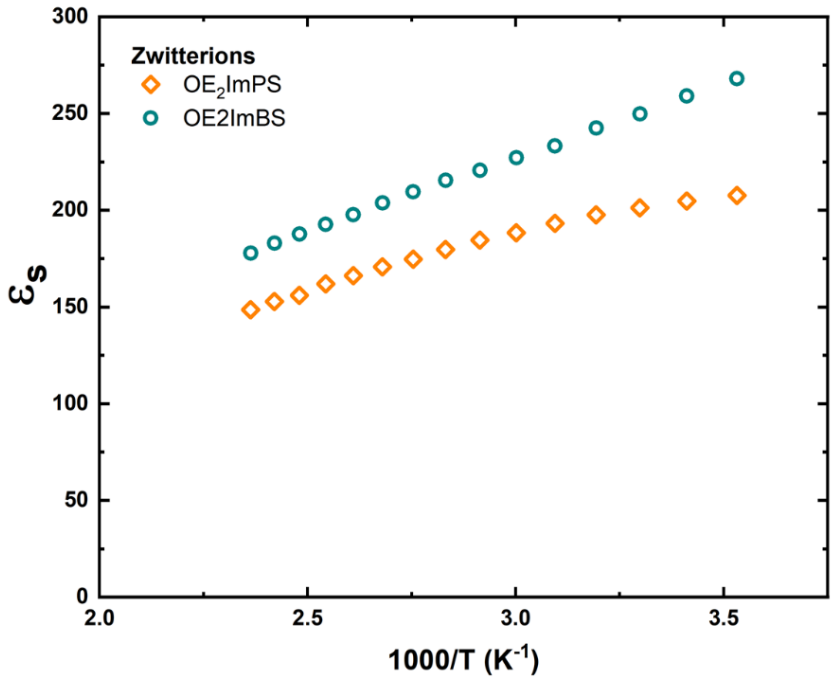

Figure 24. Static dielectric constants with respect to temperature for synthesized OE_2Im sulfonate zwitterions.

The static dielectric constants are exceptionally high for the synthesized **OE_2Im** sulfonate zwitterions and could be measured at and below room temperature due to the low T_g of the zwitterions. ε_s decreases with temperature due to thermal randomization of the freely rotating dipoles; more electric charge is dissipated at high temperature due to this random motion. The dielectric constants are not provided below the glass transition since dipole rotation no longer contributes to ε_s when the zwitterions become frozen. The **OE_2ImPS** sample began to relax at 0 °C, so the datum is not provided in Table 4. The ε_s values for **OE_2ImBS** are consistently about 30 units higher than **OE_2ImPS** due to the larger dipole in the butyl sultone zwitterion. Since the static dielectric constant is a measure of a material's polarizability, zwitterions with larger dipoles would be expected to have higher static dielectric constants.

2.4 Conclusions

Polyelectrolytes have received attention as potential alternatives to conventional lithium-ion batteries which are dangerous and bulky. While polymers provide high energy density, chemical stability, and robust mechanical properties, they have considerably lower ionic conductivities than conventional battery electrolytes. Zwitterions with high dielectric constants have been shown to dramatically increase ionic conductivity by enhancing ion dissociation from the polymer backbone. Low-melting temperature zwitterions may be especially useful since they avoid complications caused by raising the glass transition temperature of the conductive polymer system during addition of solid molecules. It is also possible to directly measure the static dielectric constant, ε_s, of the pure liquid zwitterion at room temperature. We have successfully synthesized two imidazolium sulfonate zwitterions, **OE$_2$ImPS** and **OE$_2$ImBS**, the latter being a novel molecule, which display glass transitions well below room temperature and have exceptionally high static dielectric constants. These findings suggest that the synthesized zwitterions will be very effective at increasing ionic conductivity in polyelectrolytes. It will be necessary to continue this research by incorporating the **OE$_2$ImPS** and **OE$_2$ImBS** zwitterions into polyelectrolyte systems to further test this hypothesis.

Moving forward, it will also be useful to complete the synthesis of **OE$_2$Im(iPr-OP)** to analyze the effect of a phosphate anionic functionality on the glass transition temperature and dielectric constant. Successful synthesis of the isopropyl variant of the **OE$_2$Im** phosphate zwitterion will also allow for exploration into the effect of alcohols with other alkyl, aryl, or olefinic substituents on the glass transition and static dielectric constant of the zwitterion. The most promising route forward with the synthesis is to investigate reverse-phase liquid chromatography for purification of the crude cyclic phosphate precursor.

2.5 Experimental

All glassware was dried in a 110 °C oven before use. THF was purified on a JC Meyer solvent system. All other chemicals were purchased from Sigma-Aldrich and used without further purification. **OE_2Im** and derivatives were prepared according to a procedure developed by Yoshizawa-Fujita et al.[63] The synthesis of **iPr-OP** was modeled after a procedure previously reported by Hu and Emrick.[66]

1-(2-(2-Methoxyethoxy)ethyl)-1H-imidazole (OE_2Im). Solutions of 1H-imidazole (8.32 g, 122.2 mmol) in THF (40 mL) and NaH (10.44 g, 261.0 mmol) in THF (30 mL) were prepared. The imidazole solution was added dropwise to NaH solution under flow of N_2 to yield vigorous bubbling. After stirring the reaction mixture for 24 h, 1-bromo-2-(2-methoxyethoxy)ethane (16 mL, 118.9 mmol) was added dropwise under flow of N_2. The reaction mixture was stirred at 70 °C for 20 h, then filtered to yield a dark red solution. The solvent was removed via rotary evaporation, then the crude product was purified by vacuum distillation. The product distilled at 120 °C and 200 mtorr as a yellow oil (12.05 g, 56.9%). ^{1}H NMR (400MHz, D_2O) δ 7.51 (s, 1H), 6.99 (d, *J* = 16 Hz, 2H), 4.09 (t, *J* = 8 Hz, 2H), 3.71 (t, *J* = 8 Hz, 2H), 3.54 (dd, *J* = 8, 4 Hz, 2H), 3.48 (dd, *J* = 8, 4 Hz, 2H), 3.34 (s, 3H).

3-(1-(2-Methoxyethoxyethyl)-1*H*-imidazol-3-ium-3-yl)propane-1-sulfonate (OE_2ImPS). To a reaction vessel, OE_2Im (2.0 g, 11.7 mmol), propane sultone (1.4 g, 11.4 mmol), anhydrous MeCN (2.5 mL) were added. The reaction mixture was sparged with argon for 30 min, then stirred at 55 °C for 5 days. The mixture was cooled, washed with Et_2O (3x10 mL), then dried *in vacuo* at 50 °C for 16 h to yield the product as a highly viscous brown oil (2.42 g, 73.6%). ^{1}H NMR (400 MHz, D_2O) δ 8.88 (s, 1H), 7.58 (s, 2H), 4.42 (dt, *J* = 8, 8 Hz, 4H), 3.92 (t, *J* = 4 Hz,

2H), 3.96 (dd, *J* = 8, 4 Hz, 2H), 3.60 (dd, *J* = 8, 4 Hz, 2H), 3.36 (s, 3H), 2.94 (t, *J* = 4 Hz, 2H), 2.35 (p, 8 Hz, 2H).

3-(1-(2-Methoxyethoxyethyl)-1*H*-imidazol-3-ium-3-yl)butane-1-sulfonate (OE$_2$ImBS). To a reaction vessel, OE$_2$Im (2.0g, 11.7 mmol), butane sultone (1.6 g, 11.7 mmol), anhydrous MeCN (2.5 mL) were added. The reaction mixture was sparged with argon for 30 min, then stirred at 55 °C for 5 days. The mixture was cooled, washed with Et$_2$O (3x10 mL), then dried *in vacuo* at 50 °C for 16 h to yield the product as a highly viscous brown oil (2.79 g, 77.8%). ^{1}H NMR (400 MHz, D$_2$O) δ 8.86 (s, 1H), 7.56 (s, 2H), 4.41 (t, *J* = 4 Hz, 2H), 4.28 (t, *J* = 8 Hz, 2H), 3.41 (t, *J* = 6 Hz, 2H), 3.68 (dd, *J* = 8, 4 Hz, 2H), 3.59 (dd, *J* = 8, 4 Hz, 2H), 3.36 (s, 3H), 2.95 (t, *J* = 8 Hz, 2H), 2.05 (p, *J* = 8 Hz, 2H), 1.76 (p, *J* = 8 Hz, 2H).

2-Isopropyl-1,3,2-dioxaphospholane 2-oxide (iPr-OP). A solution of anhydrous isopropyl alcohol (0.83 mL, 10.88 mmol) in THF (8 mL) was prepared and immersed in a salted ice bath at -10 °C, at which point 1-methylimidazole (0.91 mL, 11.42 mmol) was added. A solution of 2-chloro-1,3,2-dioxaphospholane 2-oxide (1 mL, 10.88 mmol) in THF (3 mL) was added dropwise over a period of 15 mins. The ice bath was removed and the reaction mixture was stirred for 3.5 h at room temperature. The solution was decanted and filtered through Celite, then the solvent removed to yield a yellow liquid (1.48 g). The crude yield of **iPr-OP** was estimated using ^{1}H NMR to be 48.2%.

BIBLIOGRAPHY

(1) Gray, C. L.; Xu, P.; Rothenberger, A. J.; Koehler, S. J.; Elacqua, E.; Milosavljevic, B. H.; Mallouk, T. E. Oligomeric Ruthenium Polypyridyl Dye for Improved Stability of Aqueous Photoelectrochemical Cells. *J. Phys. Chem. C* **2020**, *124*, 3542–3550. https://doi.org/10.1021/acs.jpcc.0c00493.

(2) Jiang, C.; Moniz, S. J. A.; Wang, A.; Zhang, T.; Tang, J. Photoelectrochemical Devices for Solar Water Splitting-Materials and Challenges. *Chem. Soc. Rev.* **2017**, *46* (15), 4645–4660. https://doi.org/10.1039/c6cs00306k.

(3) Züttel, A.; Remhof, A.; Borgschulte, A.; Friedrichs, O. Hydrogen: The Future Energy Carrier. *Philos. Trans. R. Soc. A Math. Phys. Eng. Sci.* **2010**, *368* (1923), 3329–3342. https://doi.org/10.1098/rsta.2010.0113.

(4) Hashimoto, K.; Irie, H.; Fujishima, A. TiO 2 Photocatalysis: A Historical Overview and Future Prospects. *Japanese J. Appl. Physics, Part 1 Regul. Pap. Short Notes Rev. Pap.* **2005**, *44* (12), 8269–8285. https://doi.org/10.1143/JJAP.44.8269.

(5) Sivula, K.; Le Formal, F.; Grätzel, M. Solar Water Splitting: Progress Using Hematite (a-Fe 2 O 3) Photoelectrodes. *ChemSusChem* **2011**, *4*, 432–449. https://doi.org/10.1002/cssc.201000416.

(6) Sivula, K.; Van De Krol, R. Semiconducting Materials for Photoelectrochemical Energy Conversion. *Nat. Rev. Mater.* **2016**, *1* (2). https://doi.org/10.1038/natrevmats.2015.10.

(7) Li, Z.; Luo, W.; Zhang, M.; Feng, J.; Zou, Z. Photoelectrochemical Cells for Solar Hydrogen Production: Current State of Promising Photoelectrodes, Methods to Improve Their Properties, and Outlook. *Energy Environ. Sci.* **2013**, *6* (2), 347–370. https://doi.org/10.1039/c2ee22618a.

(8) Gimenez, S.; Bisquert, J. *Photoelectrochemical Solar Fuel Production: From Basic Principles to Advanced Devices.*; Springer International Publishing, 2016. https://doi.org/10.1007/978-3-319-29641-8.

(9) Li, J.; Wu, N. Semiconductor-Based Photocatalysts and Photoelectrochemical Cells for Solar Fuel Generation: A Review. *Catal. Sci. Technol.* **2015**. https://doi.org/10.1039/C4CY00974F.

(10) Chen, X.; Liu, L.; Yu, P. Y.; Mao, S. S. Increasing Solar Absorption for Photocatalysis with Black Hydrogenated Titanium Dioxide Nanocrystals. *Science (80-.).* **2011**, *331* (6018), 746–750. https://doi.org/10.1126/science.1200448.

(11) Piskunov, S.; Lisovski, O.; Begens, J.; Bocharov, D.; Zhukovskii, Y. F.; Wessel, M.; Spohr, E. C-, N-, S-, and Fe-Doped TiO2 and SrTiO3 Nanotubes for Visible-Light-Driven Photocatalytic Water Splitting: Prediction from First Principles. *J. Phys. Chem. C* **2015**, *119* (32), 18686–18696. https://doi.org/10.1021/acs.jpcc.5b03691.

(12) O'Regan, B.; Gratzel, M. A Low-Cost, High-Efficiency Solar Cell Based on Dye-Sensitized Colloidal Ti02 Films. *Nature* **1991**, *353*, 737–740. https://doi.org/10.1016/0146-5724(84)90144-4.

(13) Kakiage, K.; Aoyama, Y.; Yano, T.; Oya, K.; Fujisawa, J. I.; Hanaya, M. Highly-Efficient Dye-Sensitized Solar Cells with Collaborative Sensitization by Silyl-Anchor and Carboxy-Anchor Dyes. *Chem. Commun.* **2015**, *51* (88), 15894–15897. https://doi.org/10.1039/c5cc06759f.

(14) Swierk, J. R.; Mallouk, T. E. Design and Development of Photoanodes for Water-Splitting Dye-Sensitized Photoelectrochemical Cells. *Chem. Soc. Rev.* **2013**, *42* (6), 2357–2387. https://doi.org/10.1039/c2cs35246j.

(15) Hara, M.; Lean, J. T.; Mallouk, T. E. Photocatalytic Oxidation of Water by Silica-Supported Tris(4,4′-Dialkyl-2,2′-Bipyridyl)Ruthenium Polymeric Sensitizers and Colloidal Iridium Oxide. *Chem. Mater.* **2001**, *13* (12), 4668–4675. https://doi.org/10.1021/cm0104811.

(16) Swierk, J. R.; McCool, N. S.; Saunders, T. P.; Barber, G. D.; Mallouk, T. E. Effects of Electron Trapping and Protonation on the Efficiency of Water-Splitting Dye-Sensitized Solar Cells. *J. Am. Chem. Soc.* **2014**, *136* (21), 10974–10982. https://doi.org/10.1021/ja5040705.

(17) Hanson, K.; Brennaman, M. K.; Luo, H.; Glasson, C. R. K. K.; Concepcion, J. J.; Song, W.; Meyer, T. J. Photostability of Phosphonate-Derivatized, Ru II Polypyridyl Complexes on Metal Oxide Surfaces. *ACS Appl. Mater. Interfaces* **2012**, *4* (3), 1462–1469. https://doi.org/10.1021/am201717x.

(18) Xu, P.; McCool, N. S.; Mallouk, T. E. Water Splitting Dye-Sensitized Solar Cells. *Nano Today*. 2017. https://doi.org/10.1016/j.nantod.2017.04.009.

(19) Poddutoori, P. K.; Thomsen, J. M.; Milot, R. L.; Sheehan, S. W.; Negre, C. F. A.; Garapati, V. K. R.; Schmuttenmaer, C. A.; Batista, V. S.; Brudvig, G. W.; Van Der Est, A. Interfacial Electron Transfer in Photoanodes Based on Phosphorus(v) Porphyrin Sensitizers Co-Deposited on SnO2 with the Ir(III)Cp∗ Water Oxidation Precatalyst. *J. Mater. Chem. A* **2015**, *3* (7), 3868–3879. https://doi.org/10.1039/c4ta07018f.

(20) Kirner, J. T.; Stracke, J. J.; Gregg, B. A.; Finke, R. G. Visible-Light-Assisted Photoelectrochemical Water Oxidation by Thin Films of a Phosphonate-Functionalized Perylene Diimide plus CoOx Cocatalyst. *ACS Appl. Mater. Interfaces* **2014**, *6* (16), 13367–13377. https://doi.org/10.1021/am405598w.

(21) Li, F.; Fan, K.; Xu, B.; Gabrielsson, E.; Daniel, Q.; Li, L.; Sun, L. Organic Dye-Sensitized Tandem Photoelectrochemical Cell for Light Driven Total Water Splitting. *J. Am. Chem. Soc.* **2015**, *137* (28), 9153–9159. https://doi.org/10.1021/jacs.5b04856.

(22) Kalyanasundaram, K. Photophysics, Photochemistry and Solar Energy Conversion with Tris(Bipyridyl)Ruthenium(II) and Its Analogues. *Coord. Chem. Rev.* **1982**, *46* (C), 159–244. https://doi.org/10.1016/0010-8545(82)85003-0.

(23) Keller, S. W.; Johnson, S. A.; Brigham, E. S.; Yonemoto, E. H.; Mallouk, T. E.; Johnson, S. A. Photoinduced Charge Separation in Multilayer Thin Films Grown by Sequential Adsorption of Polyelectrolytes. *J. Am. Chem. Soc.* **1995**, *117* (51), 12879–12880. https://doi.org/10.1021/ja00156a034.

(24) Kaschak, D. M.; Lean, J. T.; Waraksa, C. C.; Saupe, G. B.; Usami, H.; Mallouk, T. E. Photoinduced Energy and Electron Transfer Reactions in Lamellar Polyanion/Polycation Thin Films: Toward an Inorganic "Leaf." *Chemtracts* **1999**, *12* (12), 857–862.

(25) Materna, K. L.; Crabtree, R. H.; Brudvig, G. W. Anchoring Groups for Photocatalytic Water Oxidation on Metal Oxide Surfaces. *Chem. Soc. Rev.* **2017**, *46* (20), 6099–6110. https://doi.org/10.1039/c7cs00314e.

(26) Ardo, S.; Meyer, G. J. Direct Observation of Photodriven Intermolecular Hole Transfer across TiO2 Nanocrystallites: Lateral Self-Exchange Reactions and Catalyst Oxidation. *J. Am. Chem. Soc.* **2010**, *132* (27), 9283–9285. https://doi.org/10.1021/ja1035946.

(27) Chen, H. Y.; Ardo, S. Direct Observation of Sequential Oxidations of a Titania-Bound Molecular Proxy Catalyst Generated through Illumination of Molecular Sensitizers. *Nat. Chem.* **2018**, *10* (1), 17–23. https://doi.org/10.1038/NCHEM.2892.

(28) De Freitas, J. N.; Nogueira, V. C.; Ito, B. I.; Soto-Oviedo, M. A.; Longo, C.; De Paoli, M.

A.; Nogueira, A. F. Dye-Sensitized Solar Cells and Solar Module Using Polymer Electrolytes: Stability and Performance Investigations. *Int. J. Photoenergy* **2006**, *2006*, 1–6. https://doi.org/10.1155/IJP/2006/75483.

(29) Krebs, F. C.; Biancardo, M. Dye Sensitized Photovoltaic Cells: Attaching Conjugated Polymers to Zwitterionic Ruthenium Dyes. *Sol. Energy Mater. Sol. Cells* **2006**, *90* (2), 142–165. https://doi.org/10.1016/j.solmat.2005.02.006.

(30) Lapides, A. M.; Ashford, D. L.; Hanson, K.; Torelli, D. A.; Templeton, J. L.; Meyer, T. J. Stabilization of a Ruthenium(II) Polypyridyl Dye on Nanocrystalline TiO2 by an Electropolymerized Overlayer. *J. Am. Chem. Soc.* **2013**, *135* (41), 15450–15458. https://doi.org/10.1021/ja4055977.

(31) Fang, Z.; Keinan, S.; Alibabaei, L.; Luo, H.; Ito, A.; Meyer, T. J. Controlled Electropolymerization of Ruthenium(II) Vinylbipyridyl Complexes in Mesoporous Nanoparticle Films of TiO2. *Angew. Chemie Int. Ed.* **2014**, *53* (19), 4872–4876. https://doi.org/10.1002/anie.201402309.

(32) Dupray, L. M.; Devenney, M.; Striplin, D. R.; Meyer, T. J. An Antenna Polymer for Visible Energy Transfer. *J. Am. Chem. Soc.* **1997**, *119* (42), 10243–10244.

(33) Moss, J. A.; Yang, J. C.; Stipkala, J. M.; Wen, X.; Bignozzi, C. A.; Meyer, G. J.; Meyer, T. J. Sensitization and Stabilization of TiO2 Photoanodes with Electropolymerized Overlayer Films of Ruthenium and Zinc Polypyridyl Complexes: A Stable Aqueous Photoelectrochemical Cell. *Inorg. Chem.* **2004**, *43* (5), 1784–1792. https://doi.org/10.1021/ic030081a.

(34) Wee, K.-R.; Brennaman, M. K.; Alibabaei, L.; Farnum, B. H.; Sherman, B.; Lapides, A. M.; Meyer, T. J. Stabilization of Ruthenium(II) Polypyridyl Chromophores on

Nanoparticle Metal-Oxide Electrodes in Water by Hydrophobic PMMA Overlayers. *J. Am. Chem. Soc.* **2014**, *136* (39), 13514–13517. https://doi.org/10.1021/ja506987a.

(35) McCool, N. S.; Swierk, J. R.; Nemes, C. T.; Schmuttenmaer, C. A.; Mallouk, T. E. Dynamics of Electron Injection in SnO2/TiO2 Core/Shell Electrodes for Water-Splitting Dye-Sensitized Photoelectrochemical Cells. *J. Phys. Chem. Lett.* **2016**, *7* (15), 2930–2934. https://doi.org/10.1021/acs.jpclett.6b01528.

(36) Lee, S.-H. A.; Zhao, Y.; Hernandez-Pagan, E. A.; Blasdel, L.; Youngblood, W. J.; Mallouk, T. E. Electron Transfer Kinetics in Water Splitting Dye-Sensitized Solar Cells Based on Core--Shell Oxide Electrodes. *Faraday Discuss.* **2012**, *155*, 165–176.

(37) Sherman, B. D.; Ashford, D. L.; Lapides, A. M.; Sheridan, M. V.; Wee, K.-R. R.; Meyer, T. J. Light-Driven Water Splitting with a Molecular Electroassembly-Based Core/Shell Photoanode. *J. Phys. Chem. Lett.* **2015**, *6* (16), 3213–3217. https://doi.org/10.1021/acs.jpclett.5b01370.

(38) Gillaizeau-Gauthier, I.; Odobel, F.; Alebbi, M.; Argazzi, R.; Costa, E.; Bignozzi, C. A.; Qu, P.; Meyer, G. J. Phosphonate-Based Bipyridine Dyes for Stable Photovoltaic Devices. *Inorg. Chem.* **2001**, *40* (23), 6073–6079. https://doi.org/10.1021/ic010192e.

(39) Evans, I. P.; Spencer, A.; Wilkinson, G. Dichlorotetrakis (Dimethyl Sulphoxide) Ruthenium (II) and Its Use as a Source Material for Some New Ruthenium (II) Complexes. *J. Chem. Sco., Dalt. Trans.* **1973**, *2*, 204–209.

(40) Schmehl, R. H.; Auerbach, R. A.; Wacholtz, W. F.; Elliott, C. M.; Freitag, R. A.; Merkert, J. W. Formation and Photophysical Properties of Tetranuclear Bipyridyl Complexes of the Type {[(Bpy)2Ru(L-L)]3Fe}. *Inorg. Chem.* **1986**. https://doi.org/10.1021/ic00234a032.

(41) Xu, P.; Gray, C. L.; Xiao, L.; Mallouk, T. E. Charge Recombination with Fractional

Reaction Orders in Water-Splitting Dye-Sensitized Photoelectrochemical Cells. *J. Am. Chem. Soc.* **2018**, *140* (37), 11647–11654. https://doi.org/10.1021/jacs.8b04878.

(42) Khazraji, A. C.; Hotchandani, S.; Das, S.; Kamat, P. V. Controlling Dye (Merocyanine-540) Aggregation on Nanostructured TiO2 Films. An Organized Assembly Approach for Enhancing the Efficiency of Photosensitization. *J. Phys. Chem. B* **1999**, *103* (22), 4693–4700. https://doi.org/10.1021/jp9903110.

(43) Matsuzaki, H.; Murakami, T. N.; Masaki, N.; Furube, A.; Kimura, M.; Mori, S. Dye Aggregation Effect on Interfacial Electron-Transfer Dynamics in Zinc Phthalocyanine-Sensitized Solar Cells. *J. Phys. Chem. C* **2014**, *118* (31), 17205–17212. https://doi.org/10.1021/jp500798c.

(44) Hanson, K.; Brennaman, M. K.; Ito, A.; Luo, H.; Song, W.; Parker, K. A.; Ghosh, R.; Norris, M. R.; Glasson, C. R. K.; Concepcion, J. J.; et al. Structure-Property Relationships in Phosphonate-Derivatized, Ru II Polypyridyl Dyes on Metal Oxide Surfaces in an Aqueous Environment. *J. Phys. Chem. C* **2012**, *116* (28), 14837–14847. https://doi.org/10.1021/jp304088d.

(45) Gao, Y.; Ding, X.; Liu, J.; Wang, L.; Lu, Z.; Li, L.; Sun, L. Visible Light Driven Water Splitting in a Molecular Device with Unprecedentedly High Photocurrent Density. *J. Am. Chem. Soc.* **2013**, *135* (11), 4219–4222. https://doi.org/10.1021/ja400402d.

(46) Hyde, J. T.; Hanson, K.; Vannucci, A. K.; Lapides, A. M.; Alibabaei, L.; Norris, M. R.; Meyer, T. J.; Harrison, D. P. Electrochemical Instability of Phosphonate-Derivatized, Ruthenium(III) Polypyridyl Complexes on Metal Oxide Surfaces. *ACS Appl. Mater. Interfaces* **2015**, *7* (18), 9554–9562. https://doi.org/10.1021/acsami.5b01000.

(47) McCool, N. S.; Swierk, J. R.; Nemes, C. T.; Saunders, T. P.; Schmuttenmaer, C. A.;

Mallouk, T. E. Proton-Induced Trap States, Injection and Recombination Dynamics in Water-Splitting Dye-Sensitized Photoelectrochemical Cells. *ACS Appl. Mater. Interfaces* **2016**. https://doi.org/10.1021/acsami.6b05362.

(48) Press release: The Nobel Prize in Chemistry 2019 https://www.nobelprize.org/prizes/chemistry/2019/press-release/ (accessed Feb 16, 2020).

(49) Li, M.; Lu, J.; Chen, Z.; Amine, K. 30 Years of Lithium-Ion Batteries. *Adv. Mater.* **2018**, *30* (33), 1–24. https://doi.org/10.1002/adma.201800561.

(50) Weber, R. L.; Ye, Y.; Schmitt, A. L.; Banik, S. M.; Elabd, Y. A.; Mahanthappa, M. K. Effect of Nanoscale Morphology on the Conductivity of Polymerized Ionic Liquid Block Copolymers. *Macromolecules* **2011**, *44* (14), 5727–5735. https://doi.org/10.1021/ma201067h.

(51) Kim, O.; Kim, H.; Choi, U. H.; Park, M. J. One-Volt-Driven Superfast Polymer Actuators Based on Single-Ion Conductors. *Nat. Commun.* **2016**, *7*, 1–8. https://doi.org/10.1038/ncomms13576.

(52) Appetecchi, G. B.; Kim, G. T.; Montanino, M.; Carewska, M.; Marcilla, R.; Mecerreyes, D.; De Meatza, I. Ternary Polymer Electrolytes Containing Pyrrolidinium-Based Polymeric Ionic Liquids for Lithium Batteries. *Journal of Power Sources*. 2010, pp 3668–3675. https://doi.org/10.1016/j.jpowsour.2009.11.146.

(53) Abraham, K. M. Li+-Conductive Solid Polymer Electrolytes with Liquid-Like Conductivity. *J. Electrochem. Soc.* **1990**, *137* (5), 1657. https://doi.org/10.1149/1.2086749.

(54) Tiyapiboonchaiya, C.; Pringle, J. M.; MacFarlane, D. R.; Forsyth, M.; Sun, J. Polyelectrolyte-in-Ionic-Liquid Electrolytes. *Macromol. Chem. Phys.* **2003**, *204* (17),

2147–2154. https://doi.org/10.1002/macp.200350073.

(55) Ogata, N.; Sanui, K.; Rikukawa, M.; Yamada, S.; Watanabe, M. Super Ion Conducting Polymers for Solid Polymer Electrolytes. *Synth. Met.* **1995**, *69* (1–3), 521–524. https://doi.org/10.1016/0379-6779(94)02553-B.

(56) Tiyapiboonchaiya, C.; Pringle, J. M.; Sun, J.; Byrne, N.; Howlett, P. C.; MacFarlane, D. R.; Forsyth, M. The Zwitterion Effect in High-Conductivity Polyelectrolyte Materials. *Nat. Mater.* **2004**, *3* (1), 29–32. https://doi.org/10.1038/nmat1044.

(57) Nair, V.; Menon, R. S.; Sreekanth, A. R.; Abhilash, N.; Biju, A. T. Engaging Zwitterions in Carbon-Carbon and Carbon-Nitrogen Bond-Forming Reactions: A Promising Synthetic Strategy. *Acc. Chem. Res.* **2006**, *39* (8), 520–530. https://doi.org/10.1021/ar0502026.

(58) Chen, S.; Zheng, J.; Li, L.; Jiang, S. Strong Resistance of Phosphorylcholine Self-Assembled Monolayers to Protein Adsorption: Insights into Nonfouling Properties of Zwitterionic Materials. *J. Am. Chem. Soc.* **2005**, *127* (41), 14473–14478. https://doi.org/10.1021/ja054169u.

(59) Zheng, L.; Sundaram, H. S.; Wei, Z.; Li, C.; Yuan, Z. Applications of Zwitterionic Polymers. *React. Funct. Polym.* **2017**, *118* (March), 51–61. https://doi.org/10.1016/j.reactfunctpolym.2017.07.006.

(60) Shao, Q.; Jiang, S. Molecular Understanding and Design of Zwitterionic Materials. *Adv. Mater.* **2015**, *27* (1), 15–26. https://doi.org/10.1002/adma.201404059.

(61) Yoshizawa, M.; Narita, A.; Ohno, H. Design of Ionic Liquids for Electrochemical Applications. *Aust. J. Chem.* **2004**, *57* (2), 139–144. https://doi.org/10.1071/CH03240.

(62) Mecerreyes, D. Polymeric Ionic Liquids: Broadening the Properties and Applications of Polyelectrolytes. *Prog. Polym. Sci.* **2011**, *36* (12), 1629–1648.

https://doi.org/10.1016/j.progpolymsci.2011.05.007.

(63) Yoshizawa-Fujita, M.; Tamura, T.; Takeoka, Y.; Rikukawa, M. Low-Melting Zwitterion: Effect of Oxyethylene Units on Thermal Properties and Conductivity. *Chem. Commun.* **2011**, *47* (8), 2345–2347. https://doi.org/10.1039/c0cc03754k.

(64) *Broadband Dielectric Spectroscopy*; Kremer, F., Schönhals, A., Eds.; Springer-Verlag Berlin Heidelberg: New York, 2003. https://doi.org/10.1007/978-3-642-56120-7.

(65) Klein, R. J. Dielectric Properties of Conductive Ionomers, Pennsylvania State University, 2007.

(66) Hu, G.; Emrick, T. Functional Choline Phosphate Polymers. *J. Am. Chem. Soc.* **2016**, *138* (6), 1828–1831. https://doi.org/10.1021/jacs.5b13156.

(67) Iwasaki, Y.; Akiyoshi, K. Design of Biodegradable Amphiphilic Polymers: Well-Defined Amphiphilic Polyphosphates with Hydrophilic Graft Chains via ATRP. *Macromolecules* **2004**, *37* (20), 7637–7642. https://doi.org/10.1021/ma049043g.

(68) Stukenbroeker, T. S.; Solis-Ibarra, D.; Waymouth, R. M. Synthesis and Topological Trapping of Cyclic Poly(Alkylene Phosphates). *Macromolecules* **2014**, *47* (23), 8224–8230. https://doi.org/10.1021/ma501764c.

(69) Kluger, R.; Covitz, F.; Dennis, E.; Williams, L. D.; Westheimer, F. H. PH-Product and PH-Rate Profiles for the Hydrolysis of Methyl Ethylene Phosphate. Rate-Limiting Pseudorotationaz. *J. Am. Chem. Soc.* **1969**, *91* (22), 6066–6072. https://doi.org/10.1021/ja01050a023.

ACADEMIC VITA

August J. Rothenberger

Education

Bachelor of Science in Chemistry | The Pennsylvania State University
Polymer Science Minor | Schreyer Honors College | Graduation Spring 2020
Humanities and Social Sciences | Victoria University of Wellington, New Zealand
Māori Language | Māori Society and Culture | Asia Studies | Study Abroad Spring 2019

Research Experience

Imidazolium Zwitterions and Copolymer Systems | Hickey Lab | May 2018 - May 2020

- Synthesized liquid zwitterions as well as ionic copolymers by RAFT polymerization
- Determined polymer composition and study conductivity metrics of polymers and zwitterions

SnO_2 Nano-Structures for CO_2 Reduction | Kauffman Lab | Dec 2018 – Feb 2019

- Synthesized SnO_2 nanoparticles and nano-spheres using sol-gel methods
- Analyzed physical and electrochemical properties of the SnO_2 nano-structures

Oligomeric Polypyridyl Dyes for Water-Splitting | Mallouk Lab | Jan 2017 – Dec 2018

- Synthesized oligomeric ruthenium dyes to enhance the efficiency of water splitting PEC cells
- Studied kinetics of lateral electron transport pathways and dye's anchoring ability to TiO_2

Alternative Li-Ion Battery Anodes | Mullins Lab | Jun 2017 – Aug 2017

- Synthesized and characterized lead oxide nanoparticles and Ge-Se microparticles
- Analyzed electrochemical properties and performance of active materials in coin cells

Teaching Experience

eBook Assistant | PSU Chemistry Dept. | Jan 2017 - Aug 2018

- Edit and illustrate GenChem eBook for use by undergraduate students in general chemistry

Organic Chemistry Tutor | PSU Chemistry Department | Aug 2018 – Dec 2018

- Enhanced students' understanding of course material by leading group tutoring sessions
- Hosted homework and exam reviews, graded exams and assignments

Campus Involvement

Nittany Chemical Society | Service Organization | Aug 2016 – May 2020

- Participate in outreach events for grade school students to promote interest in science

Apollo: THON | Service Organization | Commander (2017) | Aug 2016 – May 2020

- Raise funds to support pediatric cancer research as part of Penn State Dance Marathon
- Organized events as commander and ensured members were enthusiastic and well informed

Presentations and Publications

Co-Author: Gray, C. L.; Xu, P.; Rothenberger, A. J.; Koehler, S. J.; Elacqua, E.; Milosavljevic, B. H.; Mallouk, T. E. **Oligomeric Ruthenium Polypyridyl Dye for Improved Stability of Aqueous Photoelectrochemical Cells**. *J. Phys. Chem. C* **2020,** *124*, 3542–3550.

Presenter: **Synthesis of an Oligomeric Polypyridyl Ruthenium Dye.** Sponsors Days Poster Session. Sept 2019. State College, PA.

Co-Presenter: **Synthesis and Photophysical Characterization of 1,6-bis(hydroxymethyl)pyrene.** Chem 457 Poster Session. Dec 2018. State College, PA.

Presenter: **Synthesis of an Oligomeric Polypyridyl Ruthenium Dye.** 8th Annual Undergraduate Research Poster Symposium. Sept 2018. State College, PA

Presenter: **Synthesis of an Oligomeric Polypyridyl Ruthenium Dye.** REU Summer Symposium and Poster Session. Aug 2018. State College, PA.

Co-Presenter: **Synthesis of 2-(4-methoxyphenyl)propanoic acid from 4-methoxyphenylacetic acid via ester protected alkylation.** Chem 213M Poster Session. Apr 2018. State College, PA.

Presenter: **Lead Copper Alloys as High Capacity Anode Material for Lithium Ion Batteries.** 7th Annual Undergraduate Research Poster Symposium. Sept 2017. State College, PA.

Presenter: **Lead Copper Alloys as High Capacity Anode Material for Lithium Ion Batteries.** Summer Scholars Symposium and Poster Session. Aug 2017. Austin, TX.

Honors and Awards

John and Elizabeth Holmes Teas Scholarship ..... 2017 - 2020

- Awarded to one rising sophomore majoring in chemistry who embodies academic excellence, strong aptitude for research, and interest in chemistry

Schreyer Honors College Scholarship ..... 2016 - 2020

- Awarded to around 200 incoming freshmen with high academic potential and leadership ability upon admission to the honors college at Penn State

ORISE Professional Internship Program..... 2018 - 2019

- Competitive internship to perform research at the Department of Energy's National Energy Technology Laboratory

Evan Pugh Scholar Award..... 2019

- Awarded to juniors in the upper 0.5 percent of their class

Benkovic Summer Research Award.....2018

- Financial support granted to undergraduates conducting exceptional summer research

UT Austin Chemistry REU 2017

- Competitive program to perform research in the chemistry of materials

Eagle Scout of Troop 2, Laurel Highlands Council..... 2013

- Highest rank in the Boy Scouts of America; Eagle project involved coordination of volunteers to refurbish and repaint a caboose for the Bridgeville Area Historical Society